GENERAL DYNAMICS CONVAIR

58 p

REPORT GDC-63-137

DATE 24 June 1963

MODEL 12

[redacted]

NASA CR56536

[redacted] CCN

# AERODYNAMIC COEFFICIENTS FOR LITTLE JOE II - APOLLO BASED ON WIND TUNNEL TESTS

T-7813

PREPARED BY R. H. Chausse
for E. C. Sevigny
R.A. Schuler
R. A. Schuler
R.A. Schuler
for W. S. Zoubek

GROUP Aerodynamics

REFERENCE

APPROVED BY R.E. Strafer
R. E. Strafer
Aero Group Engineer

CHECKED BY:
R. H. Chausse
R. H. Chausse

NO. OF PAGES

NO. OF DIAGRAMS

"Available to U.S. Government Agencies and U. S. Government Contractors Only"

REVISIONS

| NO. | DATE | BY | CHANGE | PAGES AFFECTED |
|---|---|---|---|---|
| 1 | 8-9-63 | ECL | Added Addendum A ECL ark | ii, A-1 thru A-6, Page 17 |

CLASSIFICATION CHANGE

TO - UNCLASSIFIED [redacted]

By authority of T.D. No. 74-235

D. Pruitt 3/22/74

[redacted]

## TABLE OF CONTENTS



"Available to U.S. Government Agencies and U. S. Government Contractors Only"

[redacted]

[redacted]

TABLE OF CONTENTS (Cont'd.)



[redacted]

[redacted]

# AERODYNAMIC COEFFICIENTS FOR LITTLE JOE II - APOLLO BASED ON WIND TUNNEL TESTS

## SUMMARY

14D16

An analysis of Little Joe II/Apollo wind tunnel data is presented and compared to predicted information. Also, the wind tunnel data have been extrapolated theoretically where necessary to provide a complete set of aerodynamic coefficients to be used in trajectory calculations. In general, the data contained in this report agree very well with predictions. Conf. author

## INTRODUCTION

During the months of September through November of 1962, wind tunnel tests were conducted on a 0.03 scale model of the Little Joe II/Apollo configuration shown in Figure 1. These tests were run in facilities of the NASA Research Center at Langley Field, Virginia. The tests covered a range of Mach numbers from $M \cong 0$ to $M = 4.65$. A data report (Reference 1) presents this wind tunnel data without analysis.

The analysis of the data in Reference 1 is presented herein. Axial drag has been analyzed to show the effects of Mach number, angle of attack, control surface deflection, skin friction, and base pressure (power on and power off). Rigid stability derivatives are presented for the complete configuration, body alone and fins alone. Effects of fin elasticity are also discussed. Theoretical extrapolations have been made where the wind tunnel data did not cover conditions of interest so that a complete set of aerodynamic coefficients is contained in this report.

[redacted]

[redacted]

## SYMBOLS

| | | |
|---|---|---|
| $C_A$ | Axial - force coefficient, | $\frac{\text{axial force}}{q S_b}$ |
| $C_f$ | Skin friction coefficient, | $\frac{\text{skin friction}}{q S_w}$ |
| $C_h$ | Hinge - moment coefficient, | $\frac{\text{hinge moment}}{q S_c \bar{c}_c}$ |
| $C_\ell$ | Rolling - moment coefficient, | $\frac{\text{rolling moment}}{q S_b d}$ |
| $C_{M_{(REF.)}}$ | Pitching - moment coefficient, about a given reference | $\frac{\text{pitching moment}}{q S_b d}$ |
| $C_N$ | Normal - force coefficient, | $\frac{\text{normal force}}{q S_b}$ |
| $C_{p_b}$ | Base pressure coefficient, | $\frac{P_b - P_o}{q}$ |
| D | Maximum booster diameter, 12.83 ft. | |
| M | Free stream Mach Number | |
| $P_b$ | Base Pressure | |
| $P_o$ | Free stream ambient pressure | |
| $S_b$ | Booster base area, 129.3 sq ft. | |
| $S_c$ | Fin area aft of hinge line | |
| $S_w$ | Surface area exposed to airstream | |
| V | Free stream velocity, ft/sec. | |
| $X_{c.g.}$ | Center of gravity location along X axis | |
| c.g. | Center of gravity | |

[redacted]

[redacted]

## SYMBOLS (Cont'd.)

| | | |
|---|---|---|
| $\bar{c}_e$ | Mean Aerodynamic Chord of Fin aft of Hinge Line | |
| d | Maximum Booster Diameter, 12.83 ft. | |
| q | Free-stream Dynamic Pressure ($1/2\ \rho V^2$), lb/sq ft. | |
| $C_{M_q}$ | Pitch Damping Coefficient | |
| $C_{M_\alpha}$ | Pitching Moment Curve Slope | $\left(\frac{d\,C_M}{d\,\alpha}\right)$ |
| $C_{M_\delta}$ | Pitching Moment Curve Slope | $\left(\frac{d\,C_M}{d\,\delta}\right)$ |
| $C_{N_\alpha}$ | Normal Force Curve Slope | $\left(\frac{d\,C_N}{d\,\alpha}\right)$ |
| $C_{N_\delta}$ | Normal Force Curve Slope | $\left(\frac{d\,C_N}{d\,\delta}\right)$ |
| $C_{h_\alpha}$ | Hinge Moment Curve Slope | $\left(\frac{d\,C_h}{d\,\alpha}\right)$ |
| $C_{h_\delta}$ | Hinge Moment Curve Slope | $\left(\frac{d\,C_h}{d\,\delta}\right)$ |
| $C_{\ell_\alpha}$ | Rolling Moment Curve Slope | $\left(\frac{d\,C_\ell}{d\,\alpha}\right)$ |
| $C_{\ell_\beta}$ | Rolling Moment Curve Slope | $\left(\frac{d\,C_\ell}{d\,\beta}\right)$ |
| $C_{\ell_\delta}$ | Rolling Moment Curve Slope | $\left(\frac{d\,C_\ell}{d\,\delta}\right)$ |
| $\beta$ | Sideslip angle, | degrees |
| $\alpha$ | Angle of attack, | degrees |
| $\delta$ | Control surface deflection, | degrees |
| $\rho$ | Density of air, | $\frac{\text{slugs}}{\text{ft}^3}$ |

[redacted]

[redacted]

## DISCUSSION

### AXIAL DRAG ANALYSIS

The drag analysis is considered in three major parts for the full Mach number range from M = 0 to M = 5.0. These parts are:

1) A detailed breakdown of drag contributions for zero angle of attack and zero control deflection.

2) The incremental drag effect due to angle of attack.

3) The incremental drag effect due to control surface deflection.

In addition, the drag due to reaction control fairings is discussed for a range of Mach numbers from M = 0.3 to M = 1.2. Comparisons are made of the drag due to control surface deflection in pitch and roll and the drag for the vehicle in the primary and secondary pitch plane. A comparison of the full scale vehicle and wind tunnel model is also made. Full scale dimensional data are presented in Table I.

#### Drag for Zero Angle of Attack and Zero Control Deflection

The full scale drag was developed basically from the wind tunnel data. That is, the wind tunnel data was separated into its component parts, scale effects removed, and full scale corrections made. The component drag of the Little Joe II wind tunnel model is presented in Figure 2, the increments being forebody drag, base drag, and skin friction for both the tower-body combination and the fins.

Wind tunnel data for the tower-body alone (no fins) were obtained up to and including Mach 1.2 only. Thus, the total fin drag contribution was obtained by incrementing the total configuration and tower-body alone drag data up to Mach 1.2 and by theoretical calculations for the remaining Mach range. Fin wave drag was determined by supersonic swept wedge theory. The fin base pressure was extimated on a two dimensional basis (Reference 2) and compared to the experimental base pressure of the body, since both are located in the same region. The values were found to be essentially the same.

The skin friction was calculated in the classical manner based upon the turbulent skin friction coefficient for zero heat transfer (Reference 3), wind tunnel Reynolds Number per foot, reference lengths of tower-body length and fin mean aerodynamic chord length, along with the associated wetted areas to obtain the wind tunnel drag less skin friction.

[redacted]

[redacted]

The full scale drag build up was then conducted starting with the wind tunnel forebody less skin friction drag (Figure 3). To obtain the full scale skin friction, the full scale Reynolds number versus Mach number was determined from the mission E and F profiles* (Figure 4), then the associated turbulent zero heat transfer skin friction coefficients (Reference 3),and finally drag coefficients were determined based upon the proper wetted areas (vetted area ratios and skin friction coefficients are given in Table II). The full scale drag build up was continued by including full scale power-off base drag. This drag was indicated to be equal to the wind tunnel base drag (Reference 2) since the model sting support area to model base area ratio is 0.2. The power-on base drag increment was represented by a range (upper and lower limit plus a mean value) which was recommended by the NASA, Reference 4. Thus, the full scale drag build up is complete for the basic washer off configuration. For reference, a comparison of full scale forebody drag of the washer-off, washer-on, and predicted values is presented in Figure 5.

## Drag Increment Due to Angle of Attack

The effect of angle of attack on axial drag was determined by incrementing wind tunnel data directly, Figure 6. The drag increment of the forebody and the base have been presented separately, since the base drag increment is a power-off effect and would be excessive if added along with the power-on effect. In the practical range of operation, considering missions E and F ($\pm 5°$) the base pressure increment can be considered negligible.

## Drag Increment Due to Control Surface Deflection

The effect of control surface deflection on axial drag was also determined by incrementing wind tunnel data, Figures 7 - 14. Again, the increment of the forebody and base are presented separately since the base increment would be excessive for the power-on case. The base pressure increment has only been presented for the zero angle of attack case but is indicative of trends and order of magnitude for the other angles of attack, Figure 8. The remaining values can be obtained directly from Reference 1 if desired. For the practical range of operation for missions E and F ($\pm 6°$) where drag is significant, it is satisfactory to use the forebody drag as presented and neglect the small effect on power-on base drag.

## Drag Due to Reaction Control Fairings

The reaction control fairings were removed from the model in the Mach range 0.3 through 1.2. The axial drag increment was indicated to be approximately

*Mission E is a high altitude abort and Mission F is a high q abort.

[redacted]

0.0065 with the drag rise starting at Mach 0.9 and attaining a maximum increment of 0.0090 at Mach 1.2. Since these values are small the axial drag coefficient with the reaction control fairings on may be used for the uncontrolled (fixed fin) vehicle.

Drag Comparison of Control Surface Deflection in Pitch and Roll

A limited drag comparison was made of control surface deflections for pitch and roll, Table III. The comparison was made for forebody and body base at angles of attack of zero and fourteen, control surface deflections of five and ten degrees, and all Mach numbers tested. The comparison was made by incrementing the drag for the same surface deflection of a pure roll deflection with that of a pure pitch deflection. For the practical range of control surface deflection where drag is significant for missions E and F, namely, $\pm 5°$ angle of attack and $\pm 6°$ control surface deflection, the drag increment can be considered negligible.

Drag Comparison for Primary and Secondary Pitch Plane

A drag comparison was made for orientation in both the primary and secondary pitch planes from Mach 0.3 through 1.2 and an angle of attack range of -11 to +14 for zero control surface deflection. After adjusting the data to agree at zero angle of attack, the drag agreed within $\pm .0100$ for the same angle of attack. This was considered to be insignificant.

Comparison of Full Scale Vehicle and Wind Tunnel Model

The essential difference between the wind tunnel model and the full scale vehicle is the mating and end plated regions of the corrugated skin section. At stations 227 and 326, ring flanges which are perpendicular to the vehicle axis of symmetry and block the trough of each corrugation were not represented on the model. Also at stations 0 and 227, the base region of the corrugation trough of the full scale vehicle is a venting region. The venting permits relief of internal pressure of lower altitude conditions and was not represented on the model. A theoretical calculation to estimate the increased full scale drag at Mach 2 of these variations indicated the value to be approximately .0200 axial drag coefficient. Since this value was small, no correction was included.

At a later date strakes were added to the Apollo Command Module but it is felt that their effect on total vehicle drag will be negligible.

[redacted]

[redacted]

## RIGID STABILITY COEFFICIENTS

The analysis of the rigid stability coefficients has been broken down into three areas. These are (1) complete configuration, which includes the entire Little Joe II/Apollo configuration, (2) body alone, which has the fins and reaction control fairings removed, and (3) fins alone.

### Complete Configuration

Low speed (Mach near zero) values of normal force and center of pressure location are shown in Figure 15 as a function of angle of attack at zero fin deflection for values of angle of attack up to 95°. These data are useful in determining reaction control requirements during lift-off.

The normal force slope and pitching moment slope are shown in Figures 16 and 17, respectively. These data have been obtained directly from Reference 1. Since the wind tunnel data are not linear throughout the angle of attack range, $C_{N_\alpha}$ and $C_{M_\alpha}$ have been presented for that range of angles of attack when the data is linear and for an overall average slope.

The center of pressure location measured from the base is shown in Figure 16. It has been computed by using the relation

$$\left(\frac{X_{c.p.}}{D}\right)_\alpha = \frac{C_{M_\alpha}}{C_{N_\alpha}} + \frac{X_{c.g.}}{D}$$

where $C_{M_\alpha}$ is about the moment center at 2.272 diameters from the base. The range of angles of attack for which the data are linear is shown in Figure 18. Beyond this linear region the average slope should be used, but for approximate values only. If more accurate results are desired in the high angle of attack region the actual data in Reference 1 should be referred to. The predicted values of $C_{N_\alpha}$, $C_{M_\alpha}$ and $\left(\frac{X_{c.p.}}{D}\right)_\alpha$ from Reference 5 are shown on the figures and shows the data agree well with predictions.

The normal force slope, pitching moment slope and center of pressure position due to control deflection are shown in Figures 19 and 20. These data were determined from cross plots of the pitch data at various control deflections.

The rolling moment due to control deflection, $C_{\ell_\delta}$, is shown in Figure 21. $C_{\ell_\alpha}$ is zero for all Mach numbers. Since the configuration is basically symmetric $C_{\ell_\beta}$ is also zero for the entire Mach number range.

[redacted]

CONFIDENTIAL

The pitch damping coefficient $C_{M_q}$ is presented in Figures 22, 23 and 24 for respective center of gravity positions of 1.0, 1.5 and 2.0 diameters from the base, and are compared with predicted curves from Reference 5. Figure 25 shows center of gravity positions of 1.0, 1.5, 2.0, 2.5 and 3.0 diameters from the base, which covers the c.g. travel for all missions of Little Joe II. The following equation from Appendix G of Reference 6 was used to compute $C_{M_q}$.

$$C_{M_q} = \frac{-360}{\pi}\left[C_{N_{\alpha_{BODY}}}\left(\frac{X}{D}\right)^2_{BODY} + C_{N_{\alpha_{FIN}}}\left(\frac{X}{D}\right)^2_{FIN}\right]$$

where $C_{M_q}$ is in units of per radian and X is the moment arm of the applicable force.

A comparison of $C_{N_\alpha}$, $\left(\frac{X_{c.p.}}{D}\right)_\alpha$ and $C_{M_\alpha}$ between the primary and secondary configuration is shown in Figures 26 and 27. The comparison shows that rotating the vehicle to the secondary configuration increases the static stability slightly.

The configuration for the uncontrolled flights (high q abort) differs from the controlled Little Joe II configuration in that it doesn't have the reaction control fairings. Figure 28 shows that the effect of reaction control fairings is very minor.

Hinge moment characteristics $C_{h_\beta}$ and $C_{h_\alpha}$ are shown in Figure 29 and are compared with the predictions of Reference 5. $C_{h_\alpha}$ is shown for two angle of attack ranges rather than an average value, since there is a change in slope at an angle of attack of approximately $\pm 6°$ and the values of $C_{h_\alpha}$ within the range shown are generally linear. In addition, since the wind tunnel tests were run only up to a Mach number of 1.2 the curves of $C_{h_\beta}$ and $C_{h_\alpha}$ ($\alpha = 0° - \pm 6°$) have been extrapolated to coincide with the predicted value. A literature research (References 7 through 12) showed that the predicted values are a good indication of the supersonic hinge moment characteristics.

Body Alone

The body alone values of $C_{N_\alpha}$, $\left(\frac{X_{c.p.}}{D}\right)$ and $C_{M_\alpha}$ are shown in Figures 30 and 31. Subsonic and transonic values up to M = 1.2 have been obtained directly from analysis of wind tunnel data. Values from M = 1.2 to M = 5.0 have been extrapolated based on the predicted values from Reference 5, and adjusted as necessary to make the tail alone data reasonable.

CONFIDENTIAL

~~CONFIDENTIAL~~

Tail Alone

Since the tail alone was not tested in the wind tunnel, it has been necessary to calculate the fin normal force slope and center of pressure location from the data for the complete configuration and body alone configuration. The basic relations that were used are as follow:

$$\left(C_{N_\alpha}\right)_{FIN} = \left(C_{N_\alpha}\right)_{TOTAL} - \left(C_{N_\alpha}\right)_{BODY}$$

$$\left(\frac{X_{c.p.}}{D}\right)_{FIN} = \frac{\left(\frac{X_{c.p.}}{D}\right)_{TOTAL}\left(C_{N_\alpha}\right)_{TOTAL} - \left(\frac{X_{c.p.}}{D}\right)_{BODY}\left(C_{N_\alpha}\right)_{BODY}}{\left(C_{N_\alpha}\right)_{FIN}}$$

The first attempt at computing $\left(\frac{X_{c.p.}}{D}\right)_{FIN}$ resulted in a center of pressure location ahead of the fin leading edge. This was an unreasonable value because the subsonic center of pressure location should be approximately at .25 $\bar{c}$ and at about .50 $\bar{c}$ supersonically. Investigation revealed that the numbers involved were very sensitive and by making small changes in the values of $\left(C_{M_\alpha}\right)_{BODY}$ and $\left(C_{N_\alpha}\right)_{BODY}$ large changes in $\left(\frac{X_{c.p.}}{D}\right)_{FIN}$ could be realized. The body only data was then adjusted so that $\left(\frac{X_{c.p.}}{D}\right)_{FIN}$ was at a reasonable location. The body only coefficients were then rechecked with the wind tunnel data and found to be still valid. Figure 32 presents the $\left(\frac{X_{c.p.}}{D}\right)_{FIN}$ and $\left(C_{N_\alpha}\right)_{FIN}$ for the tail only.

Configuration Changes

After the wind tunnel tests had been completed two changes were made to the Little Joe II/Apollo configuration:

1. Strakes were added to the Apollo space craft.

2. The fins on Little Joe II were moved 5-1/2 inches forward.

~~CONFIDENTIAL~~

Both of these changes are destabilizing and their effect on center of pressure location was checked. The combined effect of both changes would result in .046 diameter forward shift of the missile center of pressure location. It was felt that this was still within the accuracy of the data so no adjustments were made to the analysis curves.

## AEROELASTIC EFFECTS ON STABILITY

Aeroelastic effects on the fixed fin were investigated for high q abort mission at the maximum dynamic pressure condition of 600 psf and Mach 0.9 with a fin area of 50 $ft^2$.

The lift curve slope for the inelastic case was determined from the wind tunnel data. The spanwise airload distribution was calculated by the method of Reference 13. These loads were then used in the structural elastic matrix to determine the twist and deflections of the elastic fin. The ratio of $C_{N_\alpha}$ elastic/$C_{N_\alpha}$ inelastic of the fins was determined to be 1.05. This relatively small increase due to aeroelasticity justifies the use of rigid-body coefficients.

The aeroelastic effect of the controlled fin will be investigated at a later date.

[redacted]

## REFERENCES

1. Schuler, R. A. and LeClare, G. B., "Wind Tunnel Test Data of an .03 Scale Little Joe II/Apollo Force Model," Convair Report GDC-63-025, 19 February 1963.

2. Hoerner, Sighard, "Fluid-Dynamic Drag." Published by Author, 1958.

3. Van Driest, E. R., "Turbulent Boundary Layer in Compressible Fluids," J. Aero Sc. Vol. 18, No. 3, pages 145-160. March, 1951.

4. Hondros, J. G., "Booster Base Aspiration and Choking Phenomenon for Multi-Nozzle Configurations," NASA-MSC Memorandum for Head, Dynamics Branch, 10 October 1962.

5. Laudeman, E. C., "Aerodynamic Data for Little Joe II with 316 Inch Service Module," Convair Aerodynamic Document AD-LJ-004, 25 September 1962 (Revised 25 October 1962).

6. Chin, S. S., "Missile Configuration Design," McGraw-Hill Book Company, 1961.

7. Ashby, G. C., Jr. and Fitzgerald, P. E., Jr., "Longitudinal Stability and Control Characteristics of Missile Configurations Having Several Highly Swept Cruciform Fins and a Number of Trailing Edge and Fin-Tip Controls at Mach Numbers from 2.21 to 6.01," NASA TMX-335, January 1961

8. Ulmann, E. and Smith, F., "Aerodynamic Characteristics of a 60° Delta Wing Having Half Delta Tip Control at a Mach Number of 4.04," NACA RM L55A19, April 25, 1955.

9. Stone, D. G., "Comparisons of the Effectiveness and Hinge Moments of All Moveable Delta and Flap-Type Controls on Various Wings," NACA RM L51C22, April 1951.

10. Lord, D. and Czarnecki, K., "Aerodynamic Characteristics of Several Flap-Type Trailing-Edge Controls on a Trapezoidal Wing at Mach Numbers of 1.61 and 2.01," NACA RM L54D19, June 14, 1954.

11. Boyd, J. and Pfyl, F., "Experimental Investigation of Aerodynamically Balanced Trailing-Edge Control Surfaces on an Aspect Ratio 2 Triangular Wing at Subsonic and Supersonic Speeds," NACA RM A52L04, February 13, 1953.

[redacted]

[redacted]

REFERENCES (Cont'd.)

12. Lord, D. R. and Czarnecki, K. R., "Hinge Moment Characteristics for a Series of Controls and Balancing Devices on a 60° Delta Wing at Mach Numbers of 1.61 and 2.01," NACA RM L57B01, April 12, 1957.

13. Gray, W. L. and Schenk, K. M., "A Method for Calculating the Subsonic Steady-State Loading on an Airplane With a Wing of Arbitrary Planform and Stiffness," NACA TN 3030, December 1953.

[redacted]

[redacted]

# TABLE I

## FULL SCALE DIMENSIONAL DATA

### BODY

| | |
|---|---|
| Base Area, square feet | 129.3 |
| Maximum Diameter, feet | 12.83 |
| Total Length (including escape tower), feet | 79.2 |

### FIN

| | |
|---|---|
| Total Area per fin, square feet | 50.0 |
| Mean Aerodynamic Chord, feet | 6.58 |

### CONTROL SURFACE (One)

| | |
|---|---|
| Area, square feet | 15.0 |
| Mean Aerodynamic Chord, feet | 3.19 |

[redacted]

[redacted]

## TABLE II

### WETTED AREA RATIOS

| | $S_w/S_b$ | |
|---|---|---|
| Escape Tower | 1.41 | |
| Apollo Command Module | 1.88 | |
| Service Module and Adapter | 4.14 | 19.2 |
| Little Joe II Body | 11.77 | |
| Fins | 3.57 | |

### SKIN FRICTION COEFFICIENTS

| M | $C_{f_{(BODY)}}$ Wind Tunnel | $C_{f_{(BODY)}}$ Full Scale | $C_{f_{(FINS)}}$ Wind Tunnel | $C_{f_{(FINS)}}$ Full Scale |
|---|---|---|---|---|
| .3 | .0033 | .00190 | .0053 | .00275 |
| .5 | .0030 | .00175 | .0048 | .00250 |
| .7 | .0028 | .00165 | .0045 | .00240 |
| .8 | .0029 | .00160 | .0044 | .00230 |
| .9 | .0027 | .00155 | .0043 | .00225 |
| .95 | .0027 | .00155 | .0043 | .0022 |
| 1.0 | .0028 | .00155 | .0044 | .0022 |
| 1.2 | .0027 | .00150 | .0043 | .00215 |
| 1.57 | .0027 | .00140 | .0046 | .00205 |
| 1.8 | .0027 | .00140 | .0045 | .00200 |
| 2.16 | .0025 | .00145 | .0042 | .00210 |
| 2.8 | .0023 | .00150 | .0041 | .00225 |
| 3.86 | .0020 | .00170 | .0036 | .00290 |
| 4.65 | .0018 | .00210 | .0033 | .00350 |

[redacted]

[redacted]

# TABLE III

## DRAG INCREMENT COMPARING CONTROL SURFACE DEFLECTION FOR PITCH AND ROLL

$$\Delta C_A = \left( C_{A_{ROLL}} - C_{A_{PITCH}} \right)_{\delta^\circ}$$

$C_{A_F} = C_{A_{FOREBODY}}$

$C_{A_b} = C_{A_{base}}$

| | $\delta = 5^\circ$ | | | | $\delta = 10^\circ$ | | | |
|---|---|---|---|---|---|---|---|---|
| | $\alpha = 0^\circ$ | | $\alpha = 14^\circ$ | | $\alpha = 0^\circ$ | | $\alpha = 14^\circ$ | |
| M | $\Delta C_{A_F}$ | $\Delta C_{A_b}$ | $\Delta C_{A_F}$ | $\Delta C_{A_b}$ | $\Delta C_{A_F}$ | $\Delta C_{A_b}$ | $\Delta C_{A_F}$ | $\Delta C_{A_b}$ |
| .3 | .0040 | .0090 | .0100 | .0120 | -.0400 | .0090 | .0190 | .0070 |
| .5 | .0040 | 0 | .0150 | .0100 | .0040 | .0030 | .0510 | .0020 |
| .7 | .0025 | .0015 | .0220 | .0070 | .0170 | .0020 | .0740 | .0090 |
| .8 | -.0050 | -.0010 | .0330 | .0100 | .0160 | .0010 | .0780 | .0190 |
| .9 | .0070 | .0060 | .0320 | .0190 | .0150 | -.0010 | .0810 | .0280 |
| 1.0 | .0020 | -.0100 | .0310 | .0260 | -.0040 | .0040 | .0640 | -.0090 |
| 1.2 | .0010 | .0080 | .0300 | .0030 | .0145 | .0050 | .0590 | .0030 |
| 1.57 | .0060 | 0 | .0500 | -.0050 | - | - | - | - |
| 1.8 | .0050 | 0 | .0458 | -.0020 | - | - | - | - |
| 2.16 | .0005 | 0 | .0200 | .0015 | - | - | - | - |
| 2.8 | .0015 | .0030 | .0150 | .0020 | - | - | - | - |

[redacted]

[redacted]

## LIST OF FIGURES



[redacted]

[redacted]

## LIST OF FIGURES (Cont'd.)



[redacted]

| Positive Values for Parameters | |
|---|---|
| $\alpha$ | Nose Up |
| $C_N$ | Force Up |
| $C_M$ | Nose Up |
| $C_A$ | Force Aft |
| $C_Y$ | Force to Right |
| $C_n$ | Nose Right |
| $C_l$ | Clockwise Rotation |
| $C_h$ | Trailing Edge Up |
| $\delta_{FIN}$ | Trailing Edge Down |

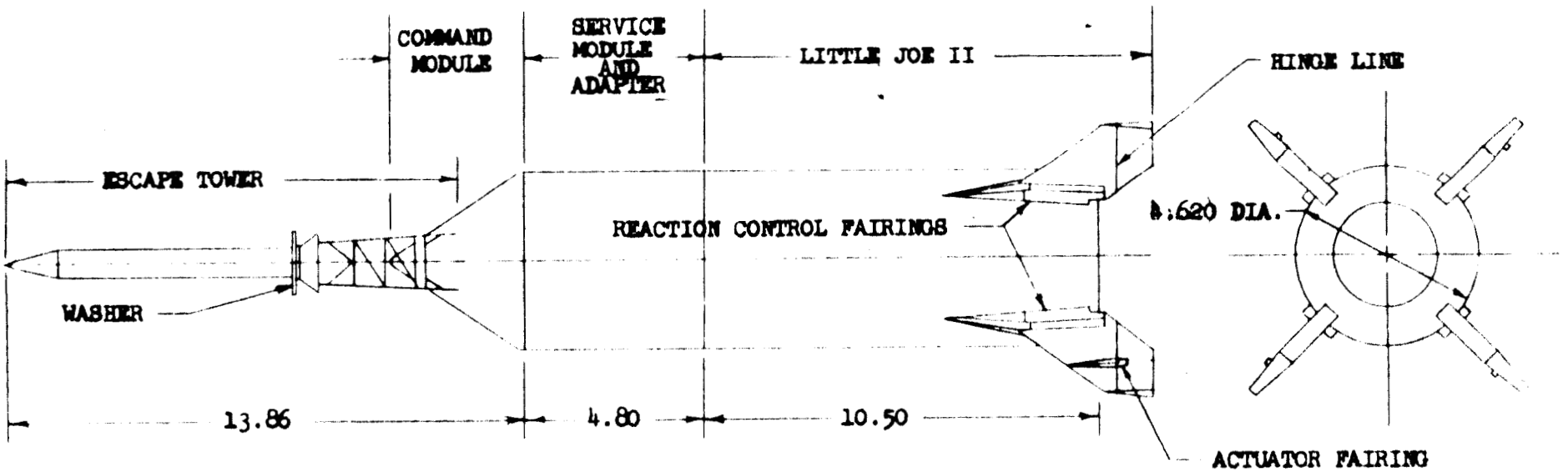


0.030 SCALE WIND TUNNEL MODEL

LITTLE JOE II - APOLLO SPACE VEHICLE



FIGURE 1

FIGURE 2

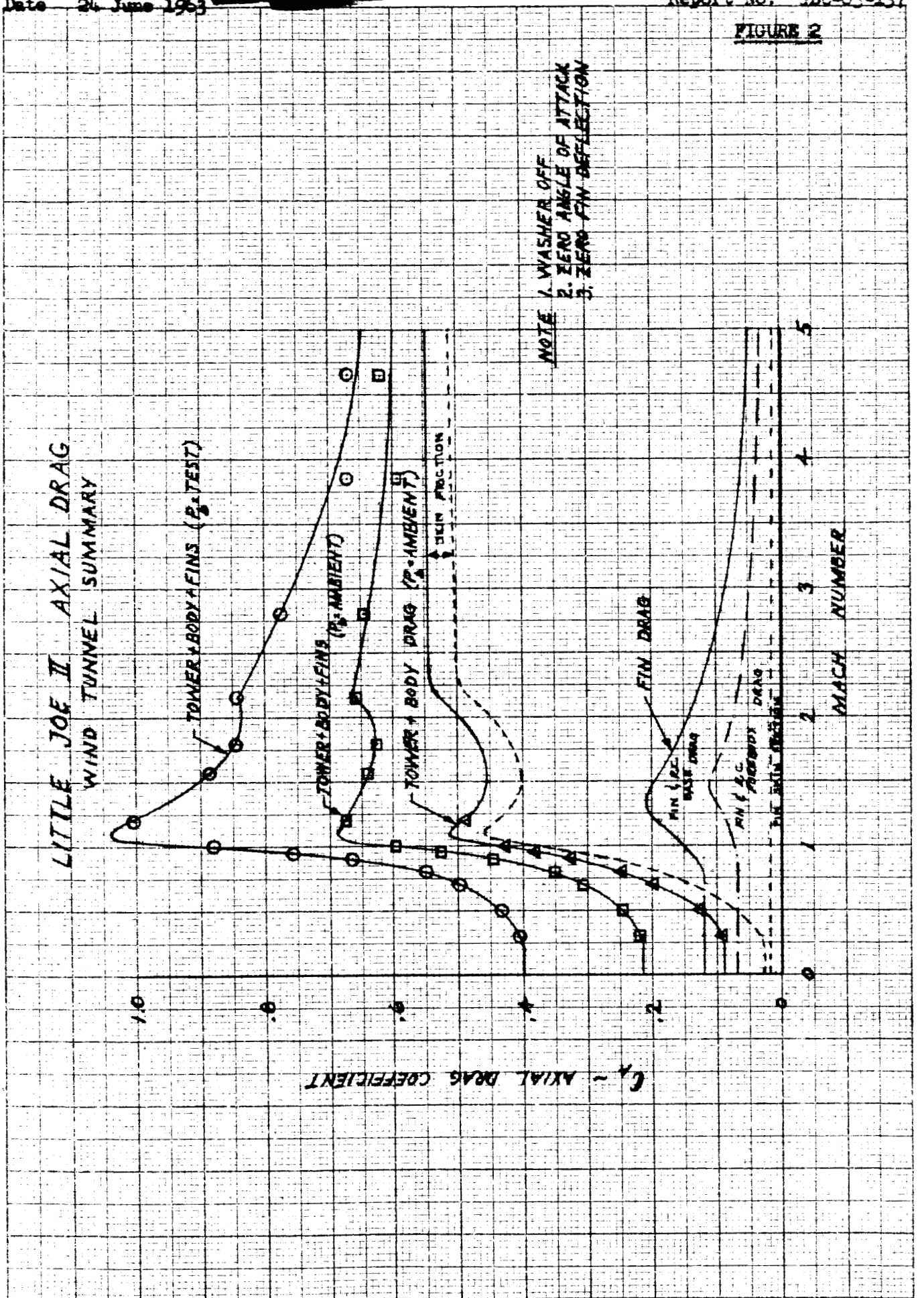
LITTLE JOE II AXIAL DRAG
WIND TUNNEL SUMMARY
NOTE 1. WASHER OFF
2. ZERO ANGLE OF ATTACK
3. ZERO FIN DEFLECTION
TOWER + BODY + FINS ($P_t$, TEST)
TOWER + BODY + FINS ($P_t$, AMBIENT)
TOWER + BODY DRAG ($P_t$ = AMBIENT)
SKIN FRICTION
FIN DRAG
FIN L.E. BASE DRAG
FIN L.E. PRESSURE DRAG
FIN SKIN FRICTION DRAG
$C_A$ - AXIAL DRAG COEFFICIENT
MACH NUMBER
1.0
.8
.6
.4
.2
0
1
2
3
4
5

FIGURE 3

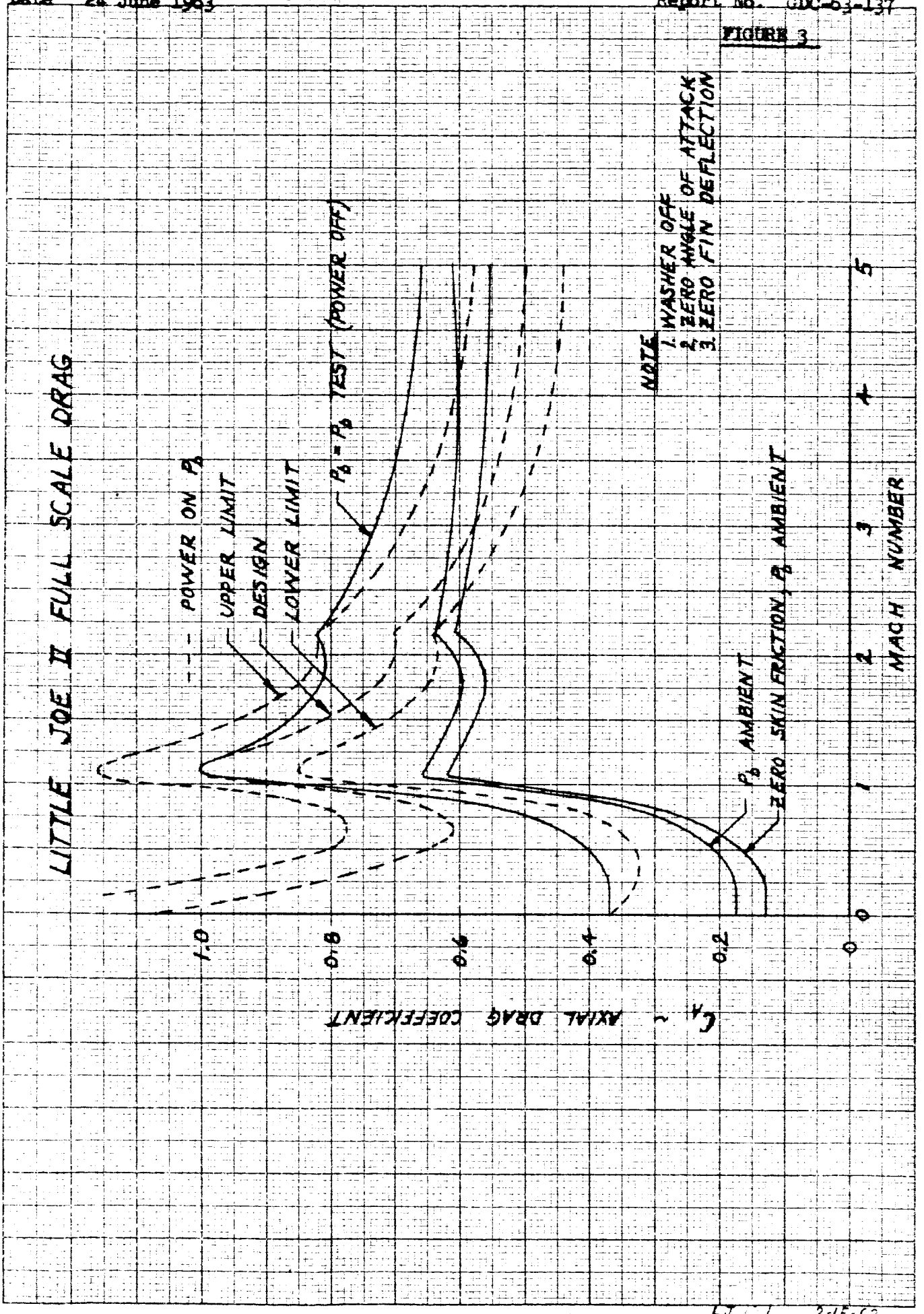


LJ - 1 2-15-63

# LITTLE JOE II FULL SCALE REYNOLDS NUMBER

FIGURE 4

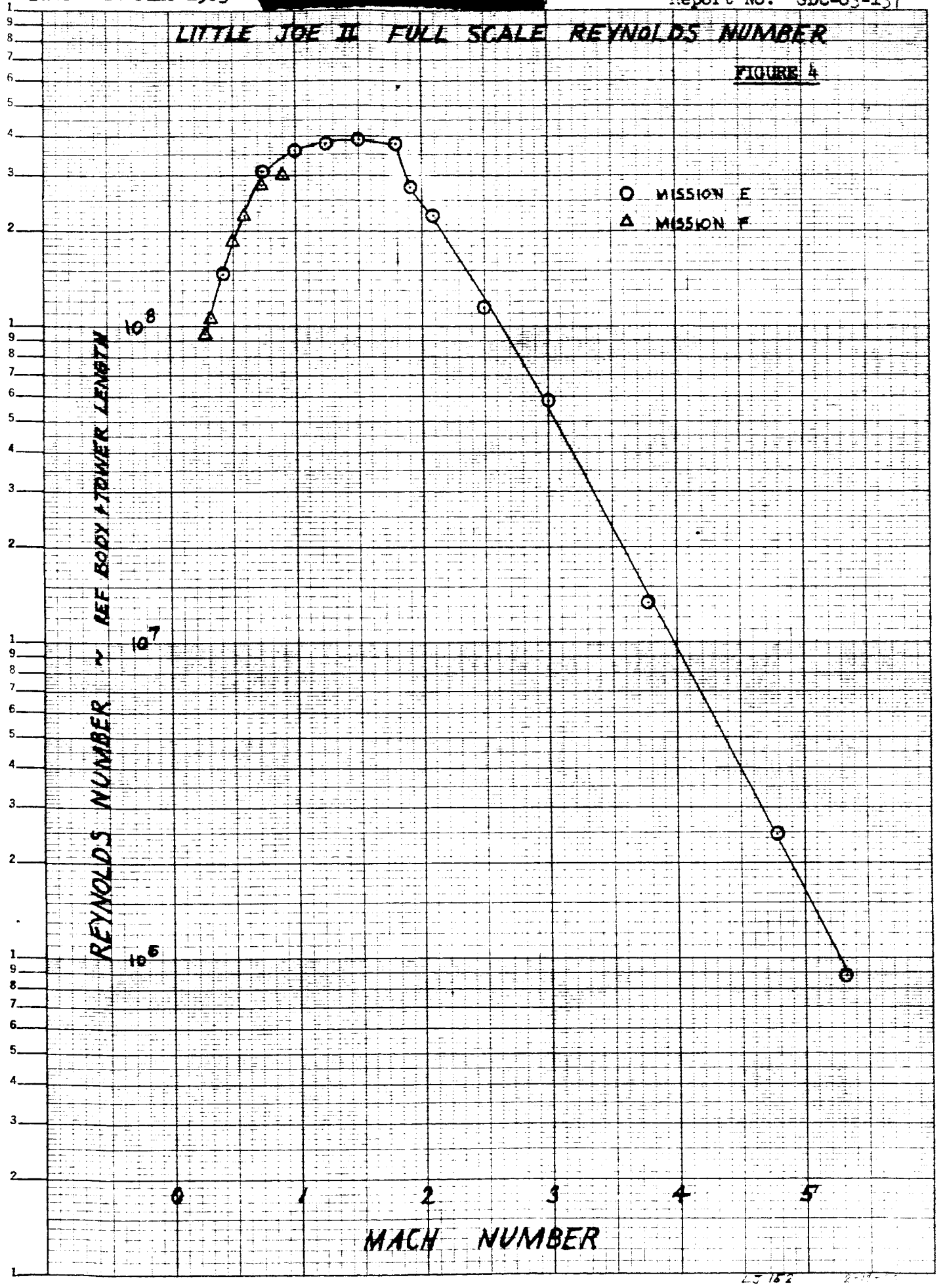


SEMI-LOGARITHMIC 359-81
KEUFFEL & ESSER CO.
4 CYCLES X 70 DIVISIONS

[redacted]

FIGURE 5

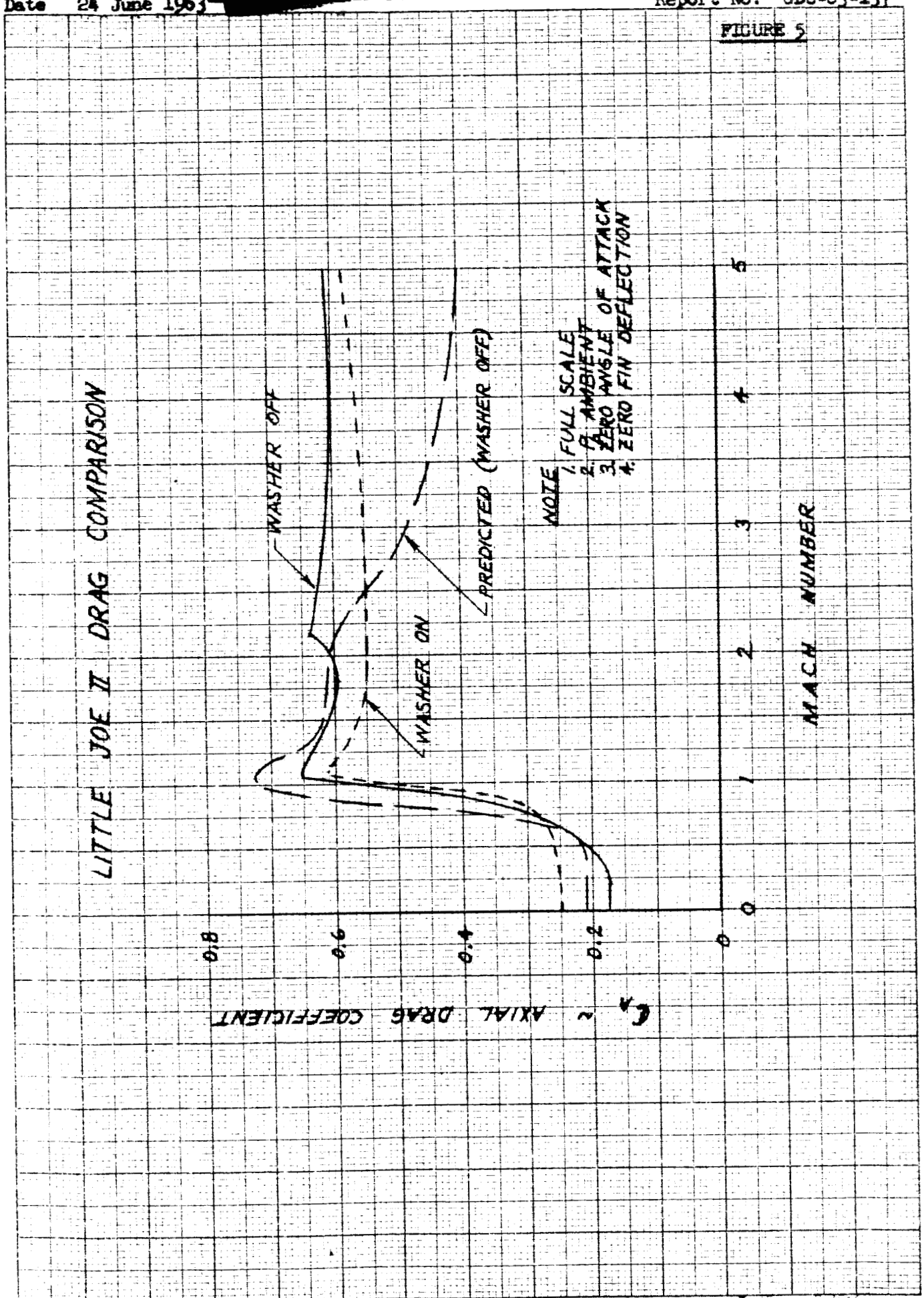
LITTLE JOE II DRAG COMPARISON
WASHER OFF
PREDICTED (WASHER OFF)
WASHER ON
NOTE
1. FULL SCALE
2. $\beta$, AMBIENT
3. ZERO ANGLE OF ATTACK
4. ZERO FIN DEFLECTION
AXIAL DRAG COEFFICIENT ~ $C_A$
MACH NUMBER
0.8
0.6
0.4
0.2
0
1
2
3
4
5
6

FIGURE 6

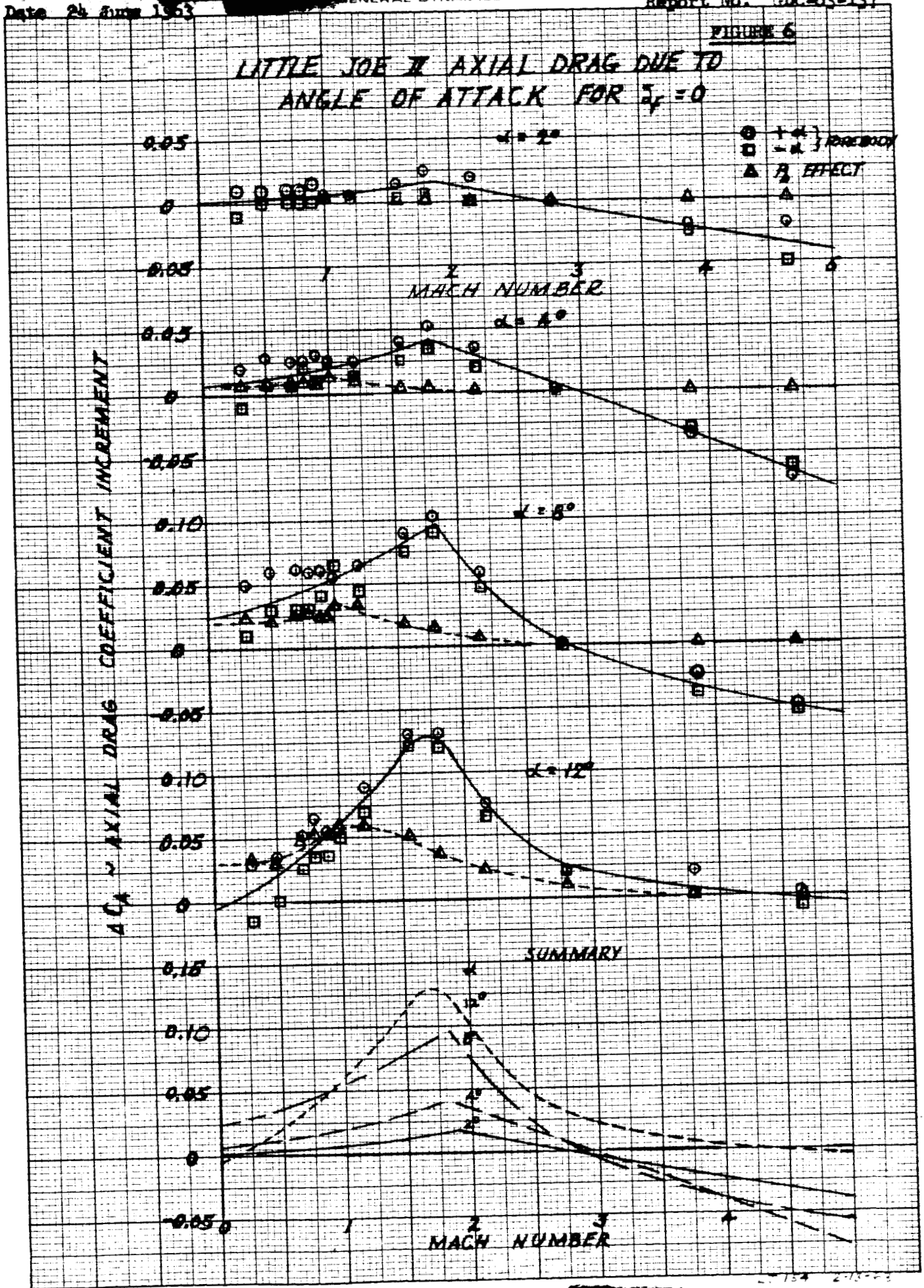
LITTLE JOE II AXIAL DRAG DUE TO ANGLE OF ATTACK FOR $\delta_f = 0$
$\alpha = 2°$
$\alpha = 4°$
$\alpha = 8°$
$\alpha = 12°$
+α } BODY
−α }
$\beta_2$ EFFECT
$\Delta C_A$ = AXIAL DRAG COEFFICIENT INCREMENT
MACH NUMBER
SUMMARY
0.05
0
-0.05
0.10
0.15
1
2
3
4

FIGURE 7

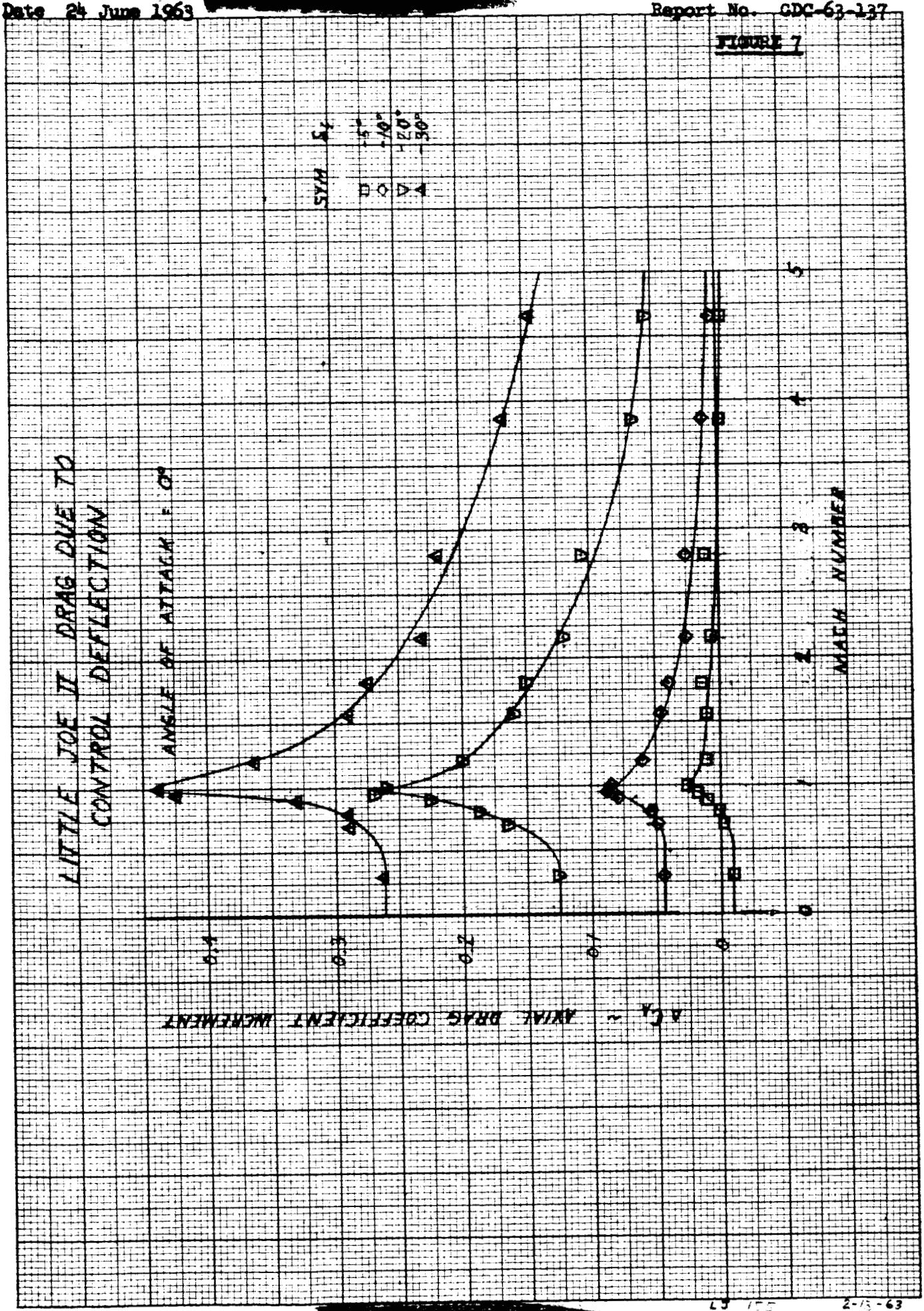

# LITTLE JOE II
## INCREMENT IN BASE DRAG DUE TO CONTROL DEFLECTION
### ANGLE OF ATTACK = 0°

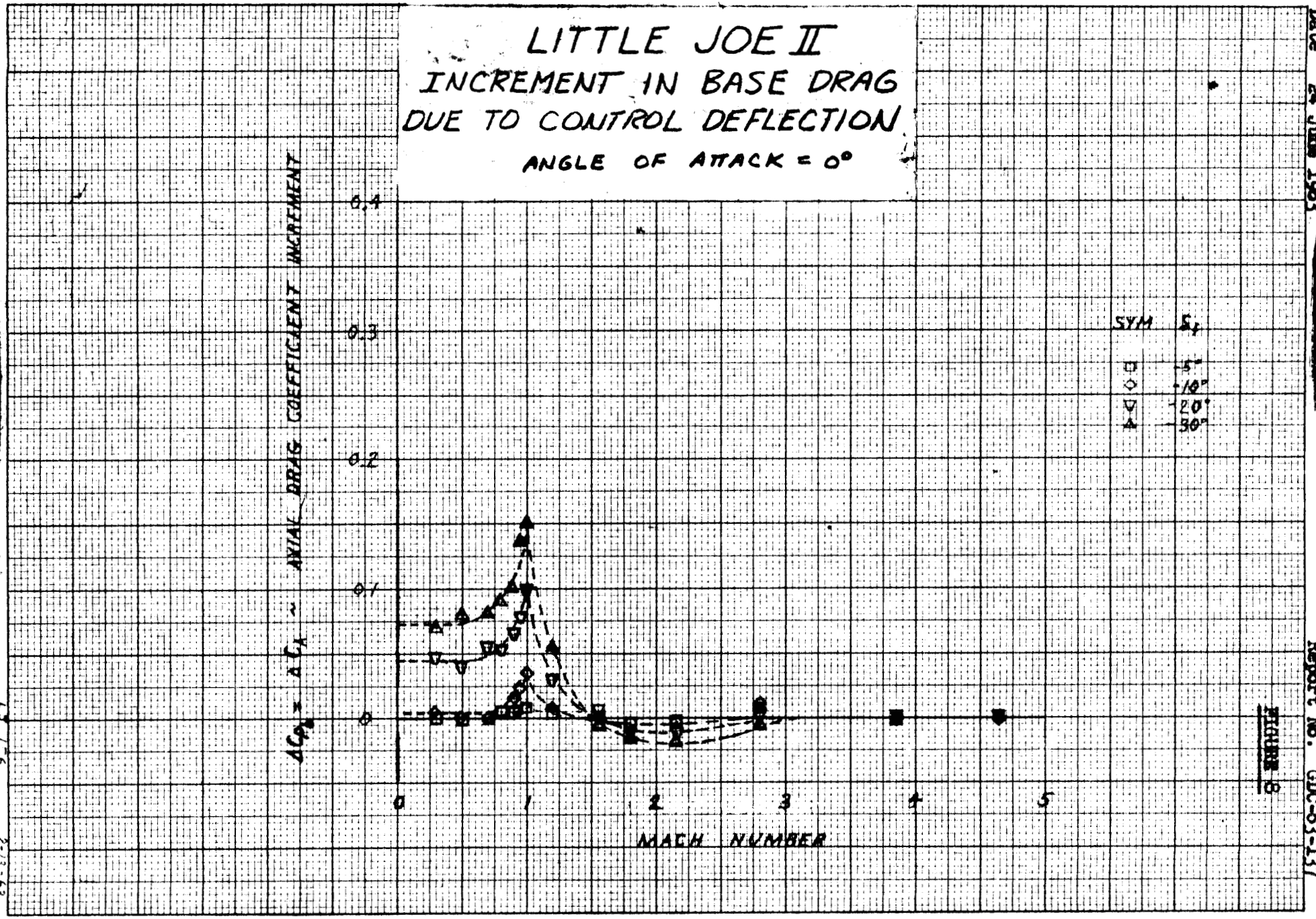


FIGURE 18

2-13-63

FIGURE 9

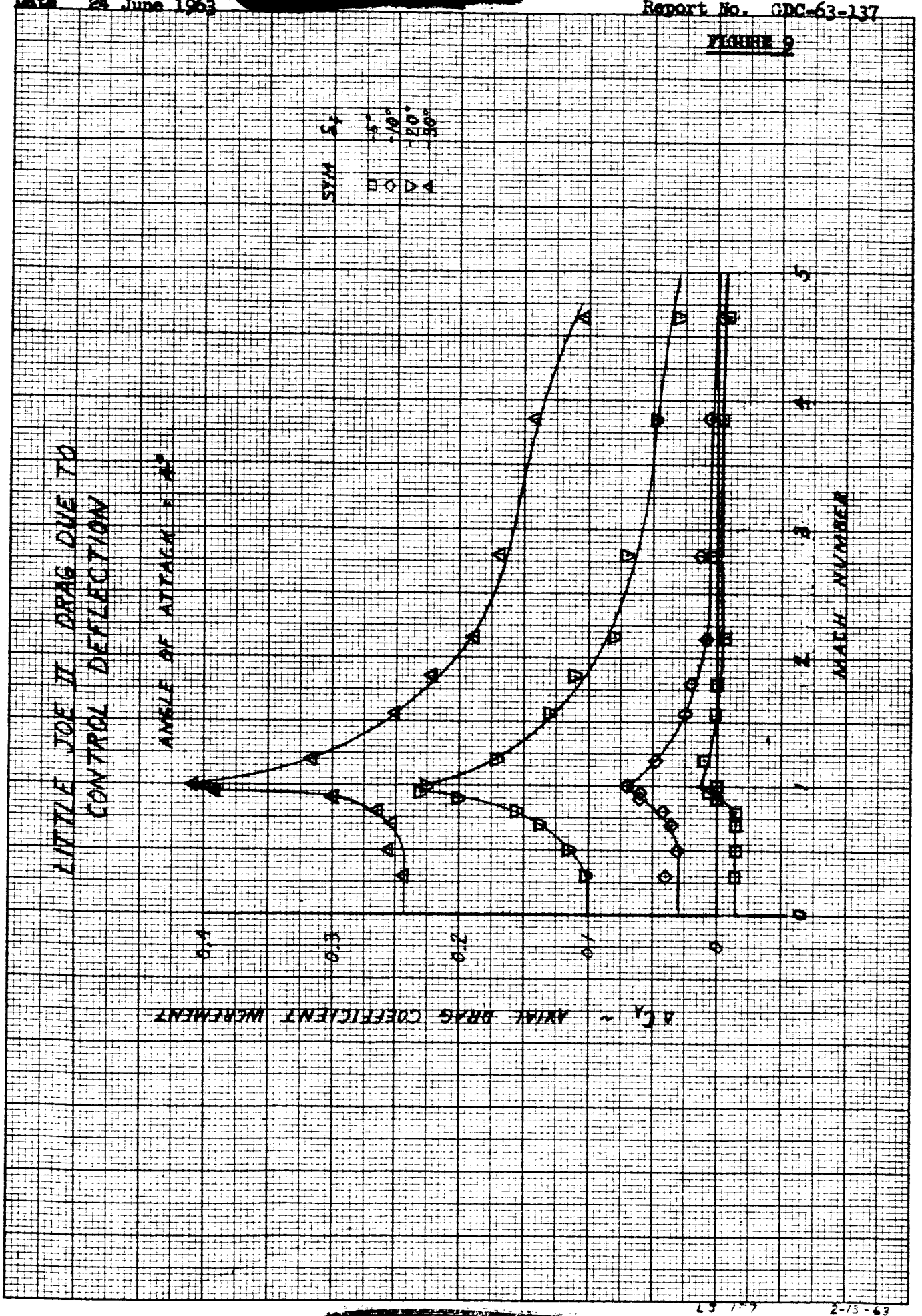

FIGURE 10

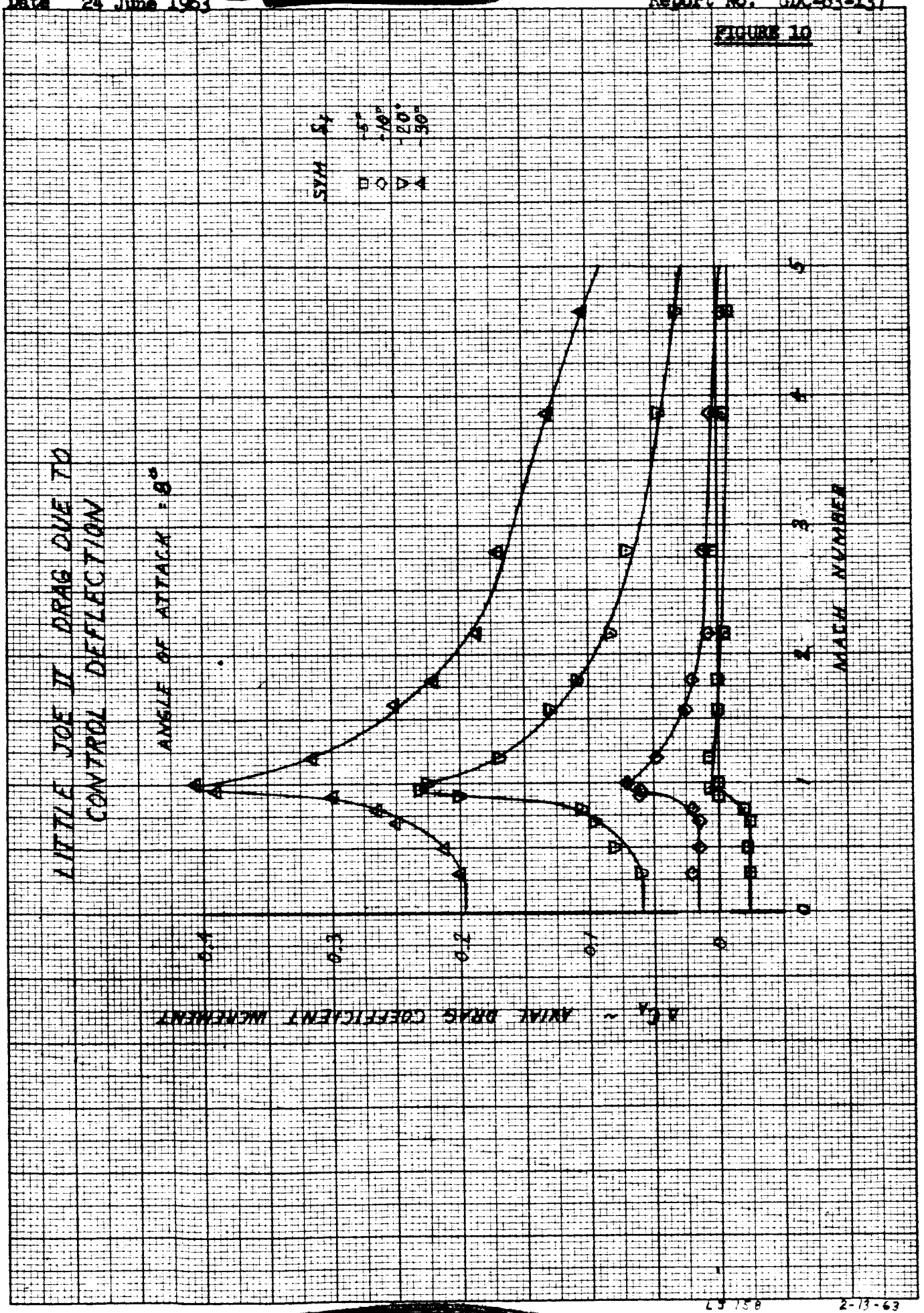






[redacted]

FIGURE 11

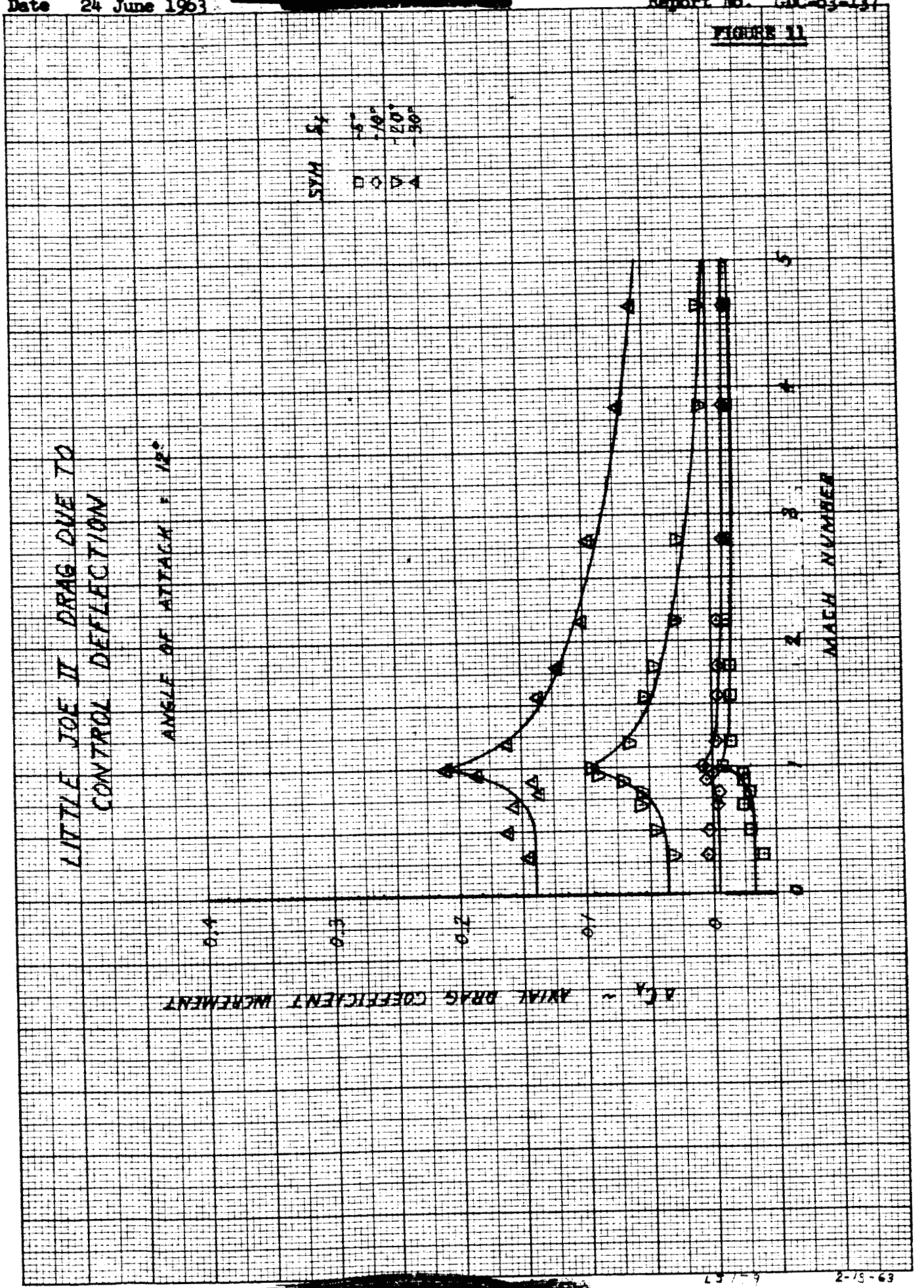

FIGURE 12

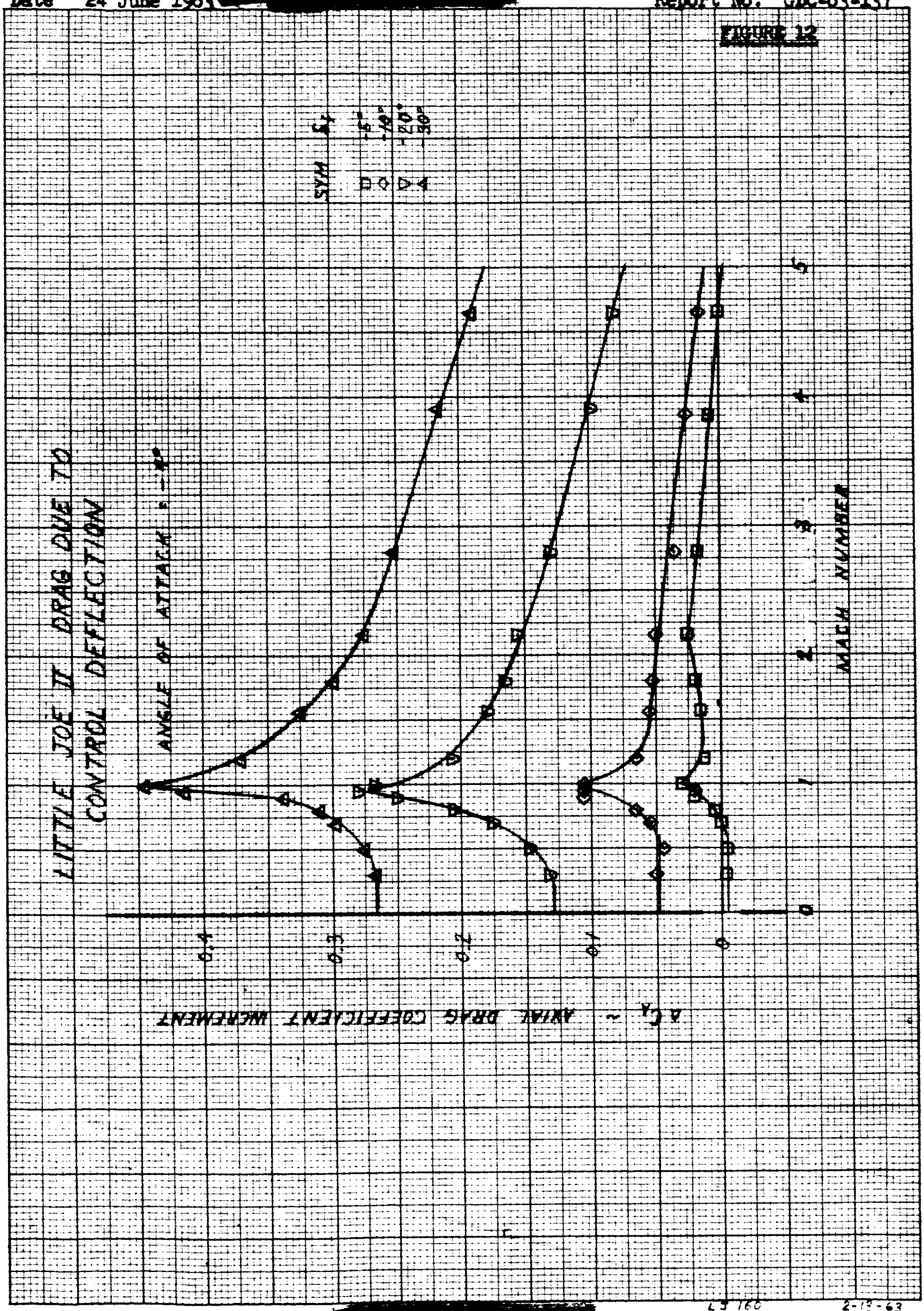


LJ 160 2-19-63

FIGURE 13

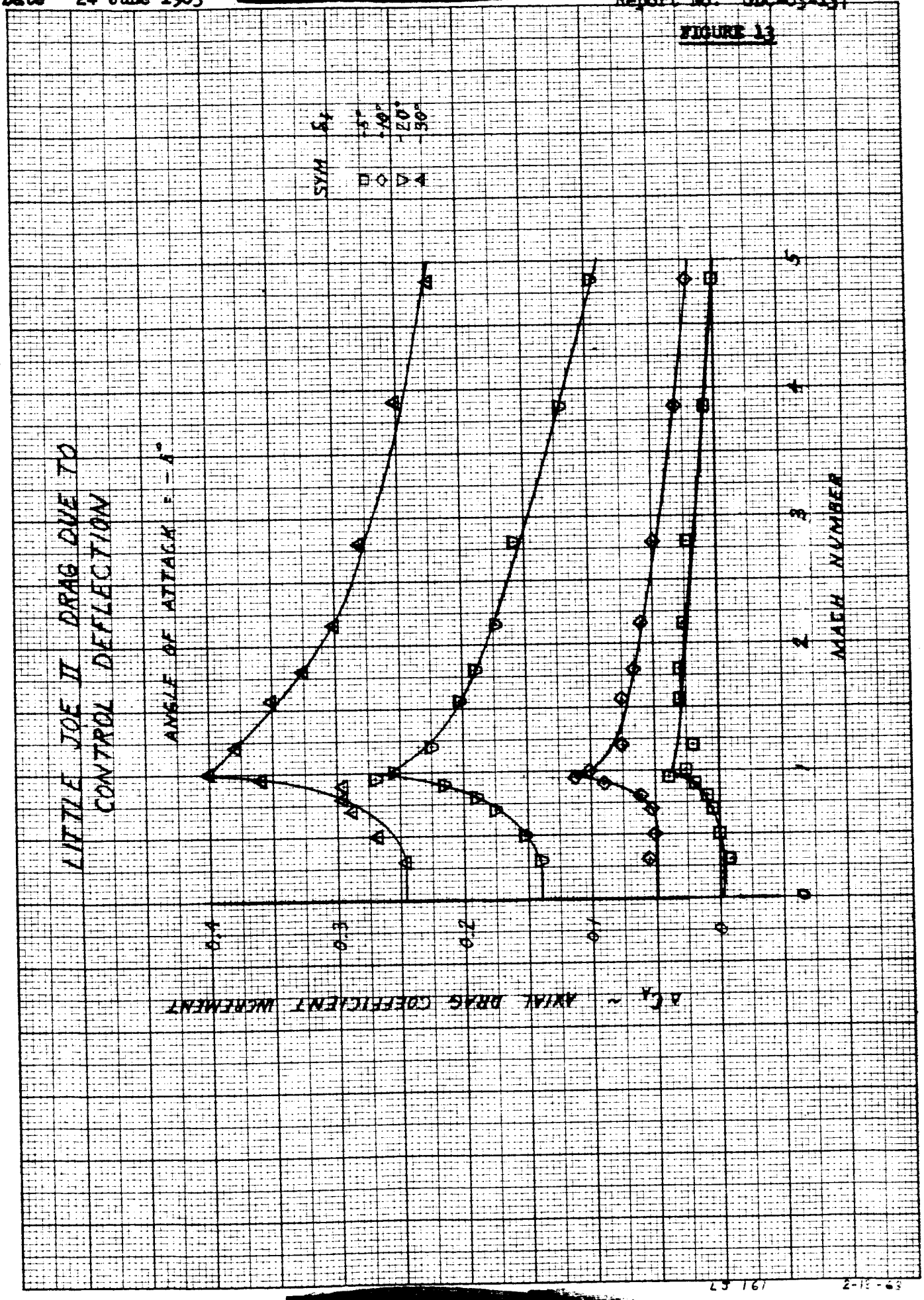

FIGURE 14

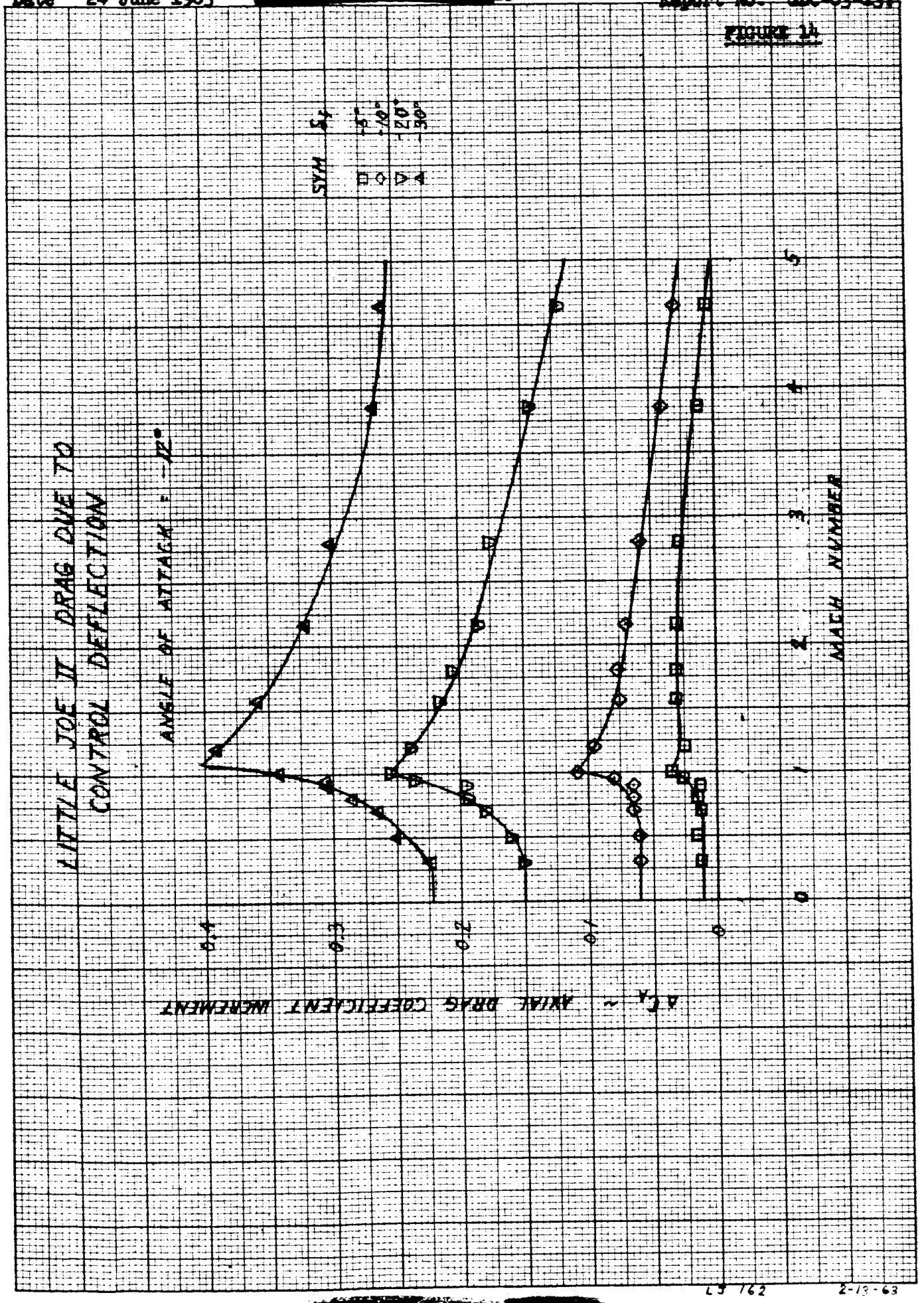




LJ 162 2-13-63

# LITTLE JOE II

FIGURE 15

## NORMAL FORCE AND CENTER OF PRESSURE LOCATION VS. ANGLE OF ATTACK

COMPLETE CONFIGURATION WITH 160 INCH SERVICE MODULE AND 50 SQ FT. FINS

$q = 14.95$ $\delta_{FIN} = 0°$

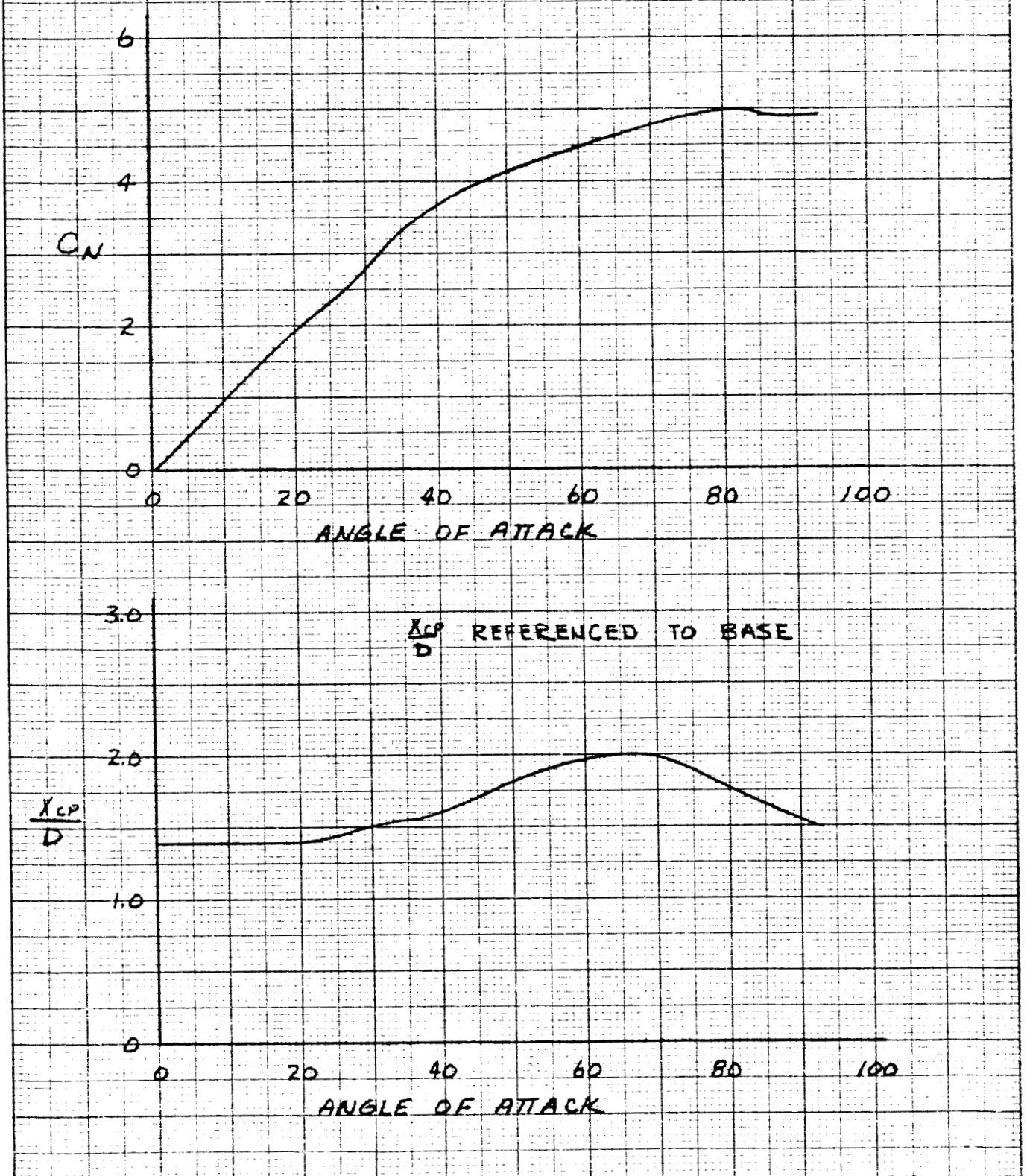

# LITTLE JOE II
## NORMAL FORCE AND CENTER OF PRESSURE LOCATION DUE TO ANGLE OF ATTACK

FIGURE 16

COMPLETE CONFIGURATION WITH 160 INCH SERVICE MODULE AND 50 SQ.FT. FINS

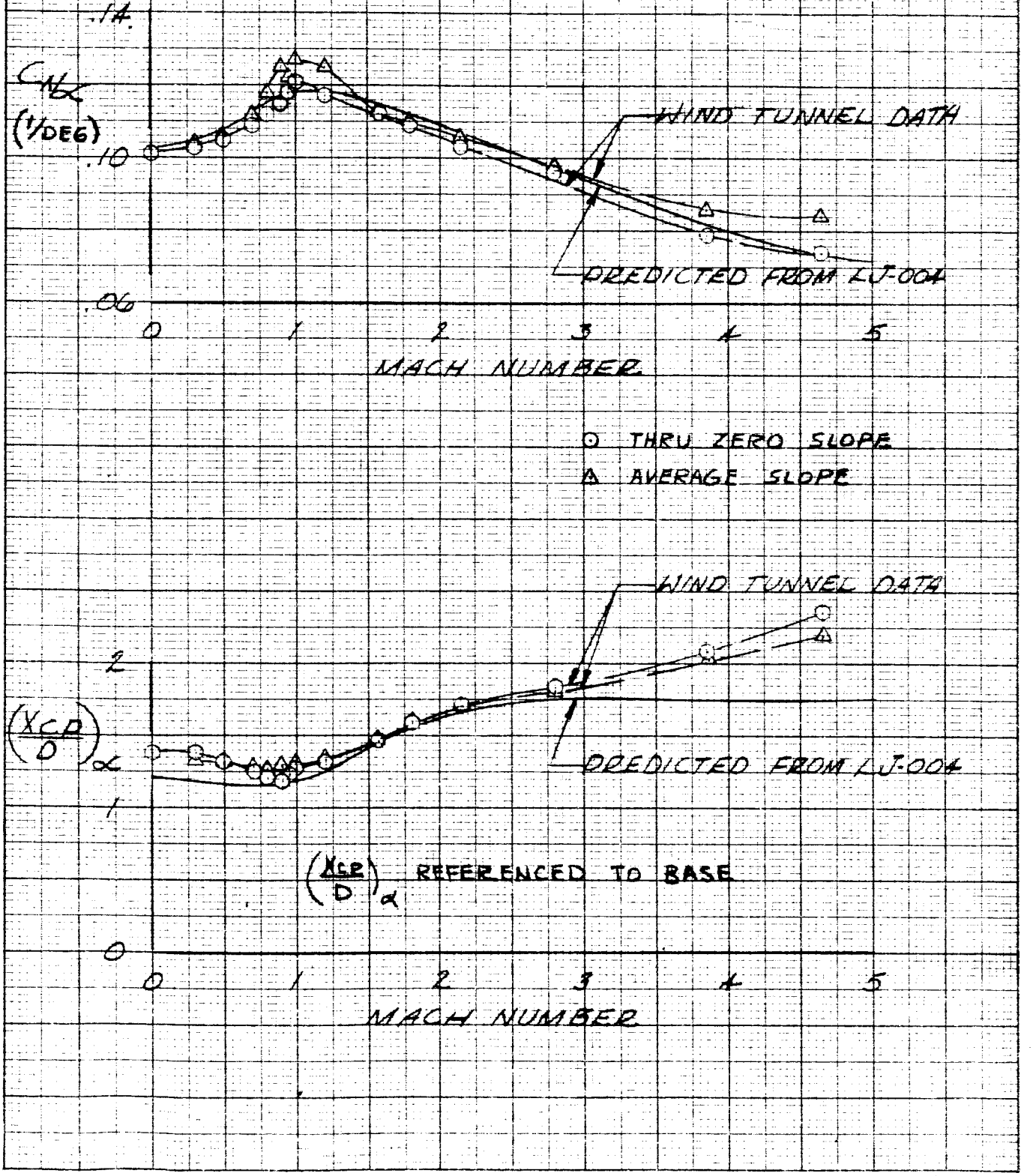

# LITTLE JOE II
## PITCHING MOMENT DUE TO ANGLE OF ATTACK

FIGURE 17

COMPLETE CONFIGURATION WITH
160 INCH SERVICE MODULE AND
50 SQ FT FINS

MOMENT REFERENCE AT 2.272 DIAMETERS FROM BASE

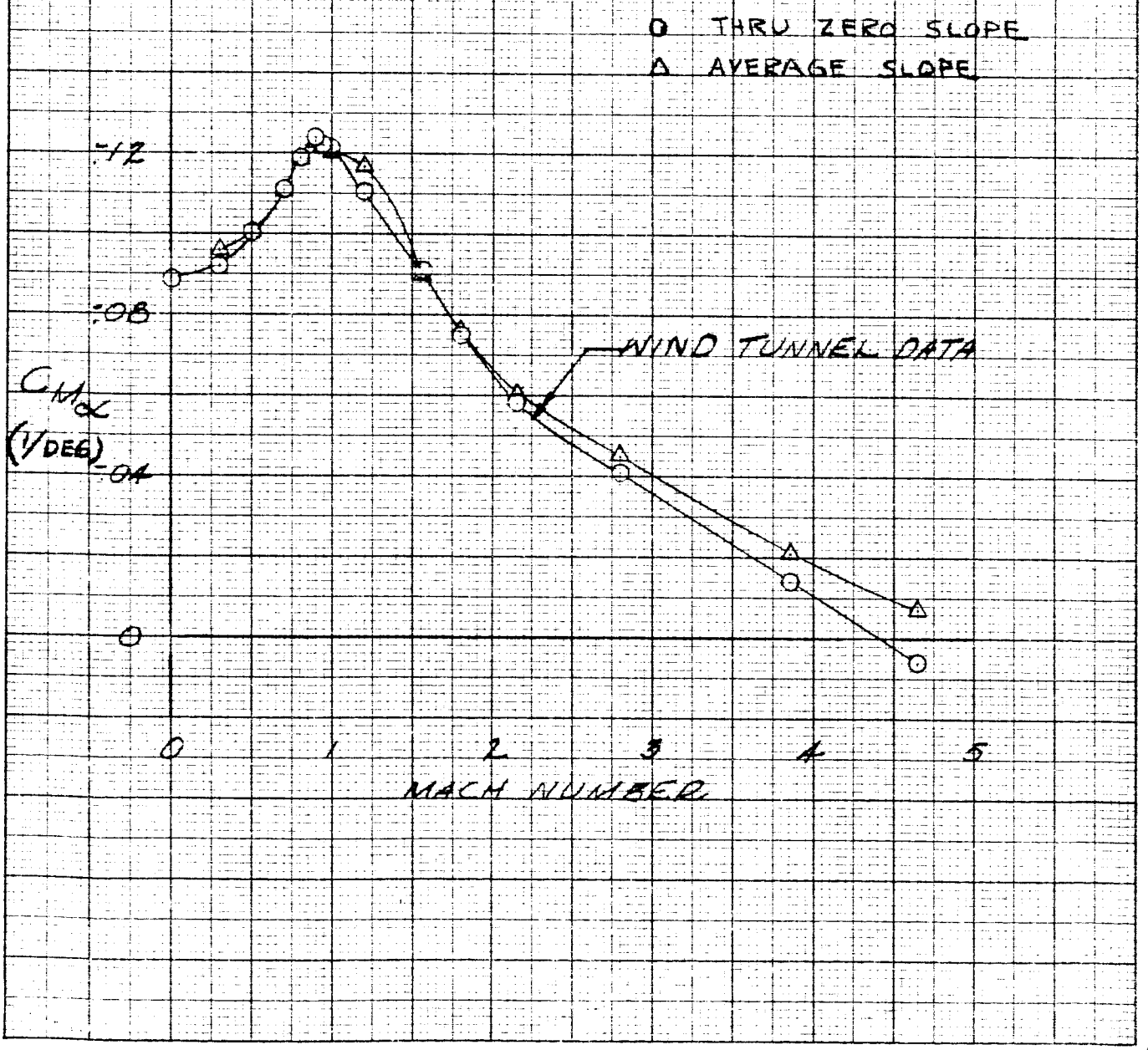

# LITTLE JOE II

FIGURE 18

## RANGE OF ANGLE OF ATTACK FOR LINEAR $C_{N_\alpha}$ & $C_{M_\alpha}$ (COMPLETE CONFIGURATION)

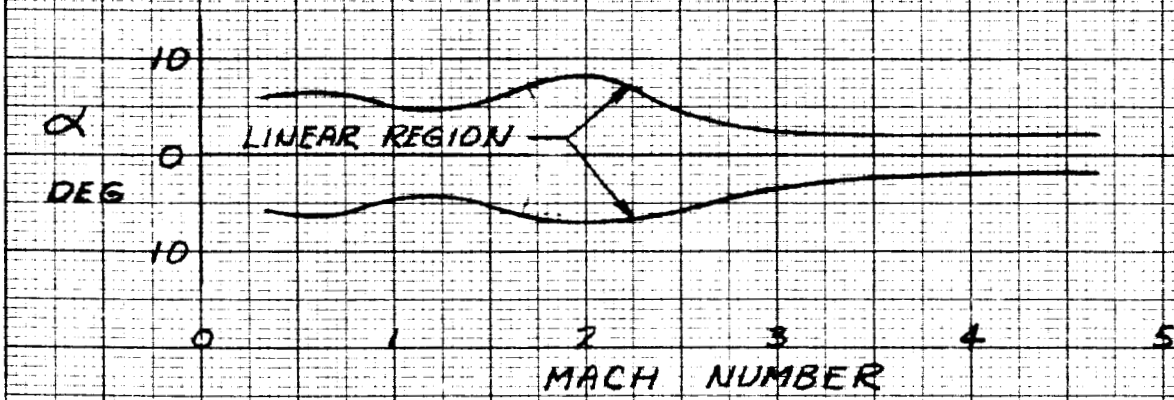

# LITTLE JOE II
## NORMAL FORCE AND CENTER OF PRESSURE LOCATION DUE TO CONTROL DEFLECTION

FIGURE 19

COMPLETE CONFIGURATION WITH 160 INCH SERVICE MODULE AND 50 SQ FT. FINS

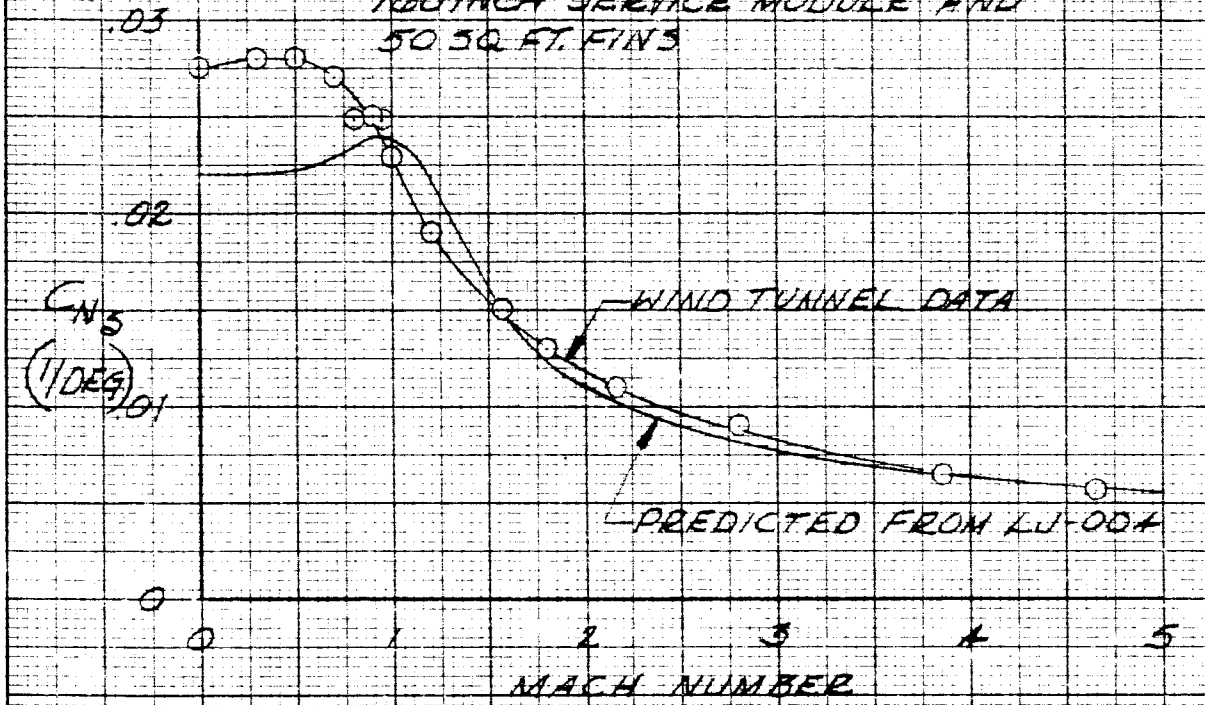


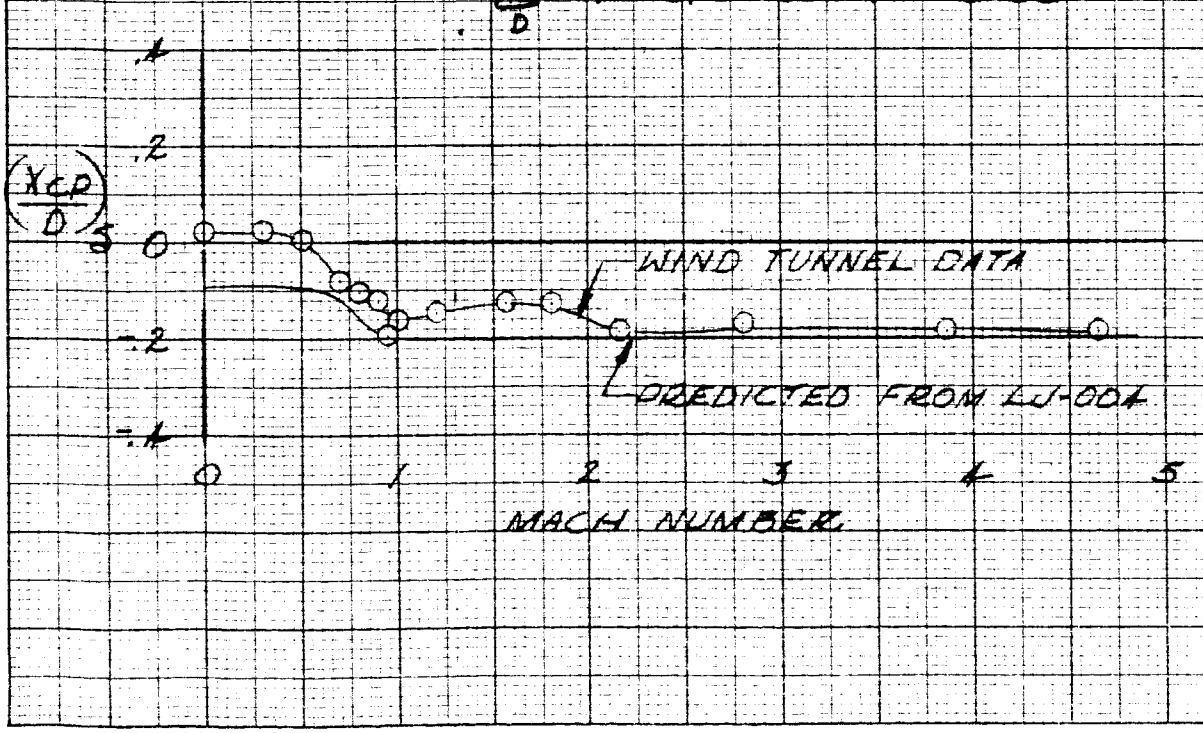

# LITTLE JOE II

FIGURE 20

## PITCHING MOMENT DUE TO CONTROL DEFLECTION

COMPLETE CONFIGURATION WITH 160 INCH SERVICE MODULE AND 50 SQ FT FINS

MOMENT REFERENCE 2.272 DIAMETERS FROM BASE

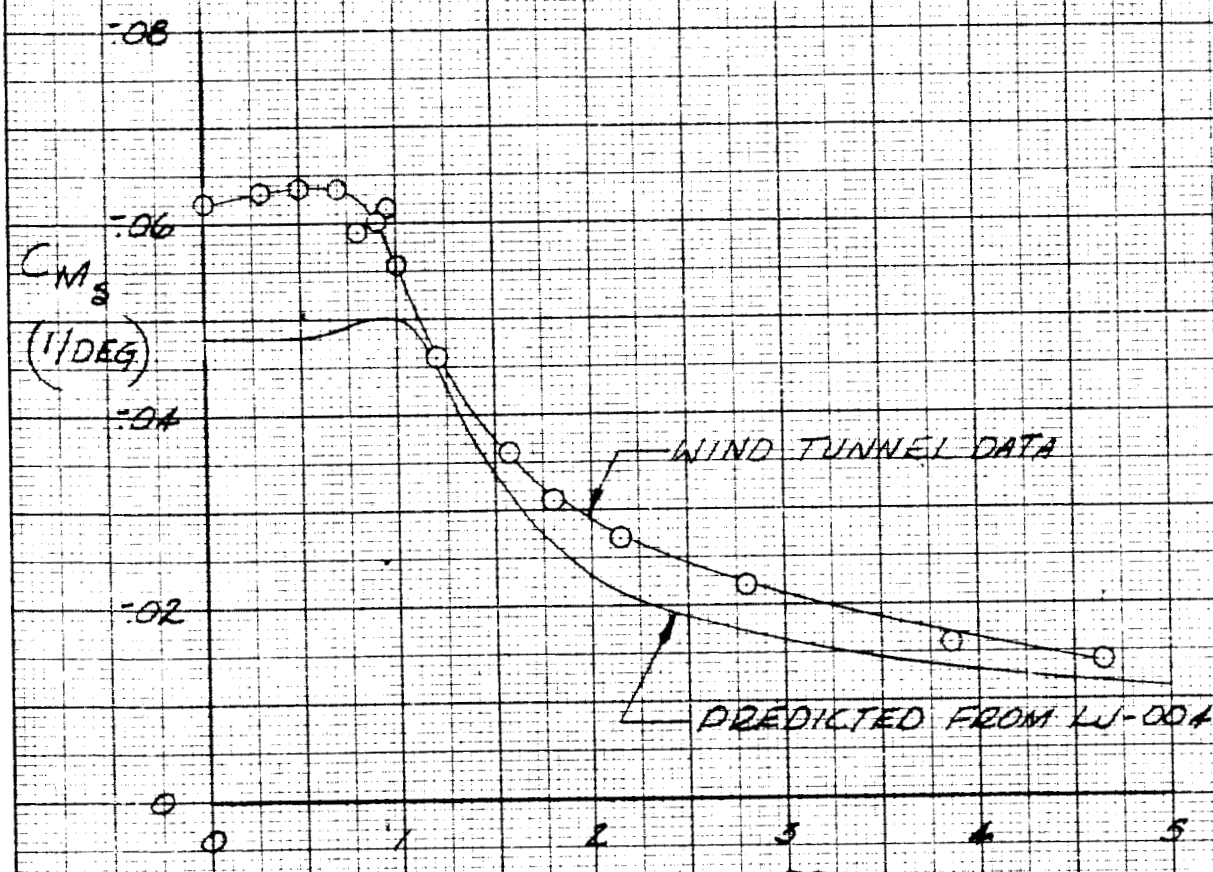




LJ-2
5/24/63

# LITTLE JOE II
## ROLL DUE TO CONTROL DEFLECTION
## (COMPLETE CONFIGURATION)

FIGURE 21

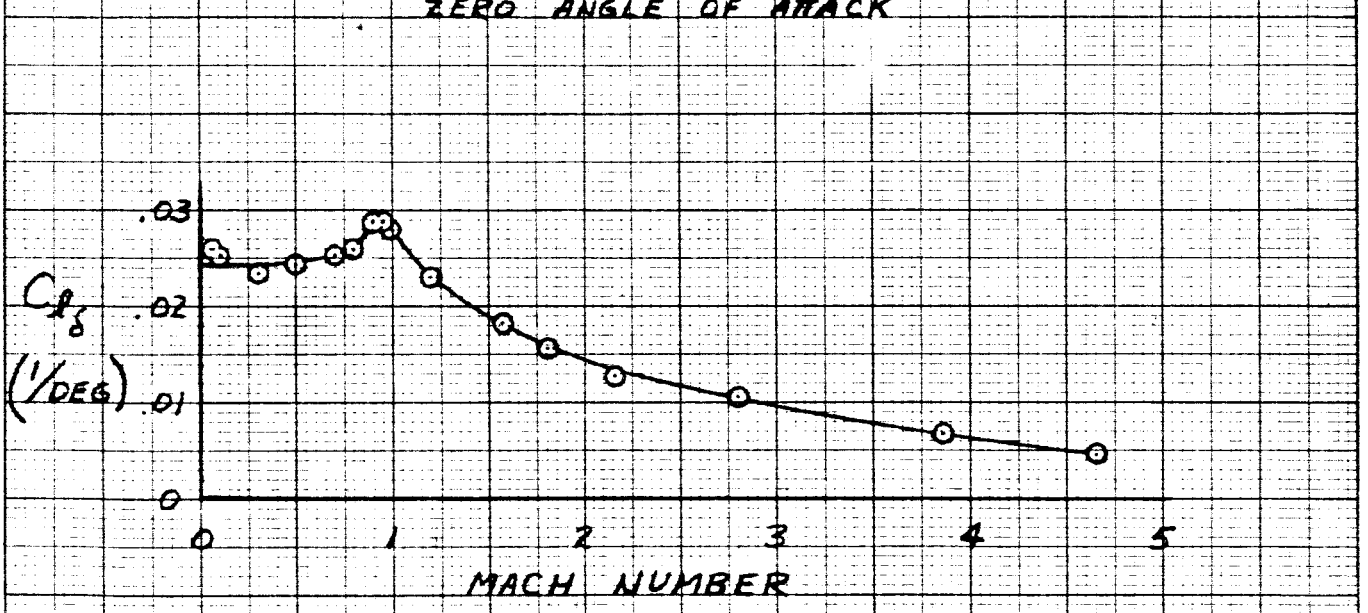

# LITTLE JOE II

FIGURE 22

## PITCHING MOMENT DUE TO PITCH RATE (COMPLETE CONFIGURATION)

C.G @ 1.0 D FROM BASE

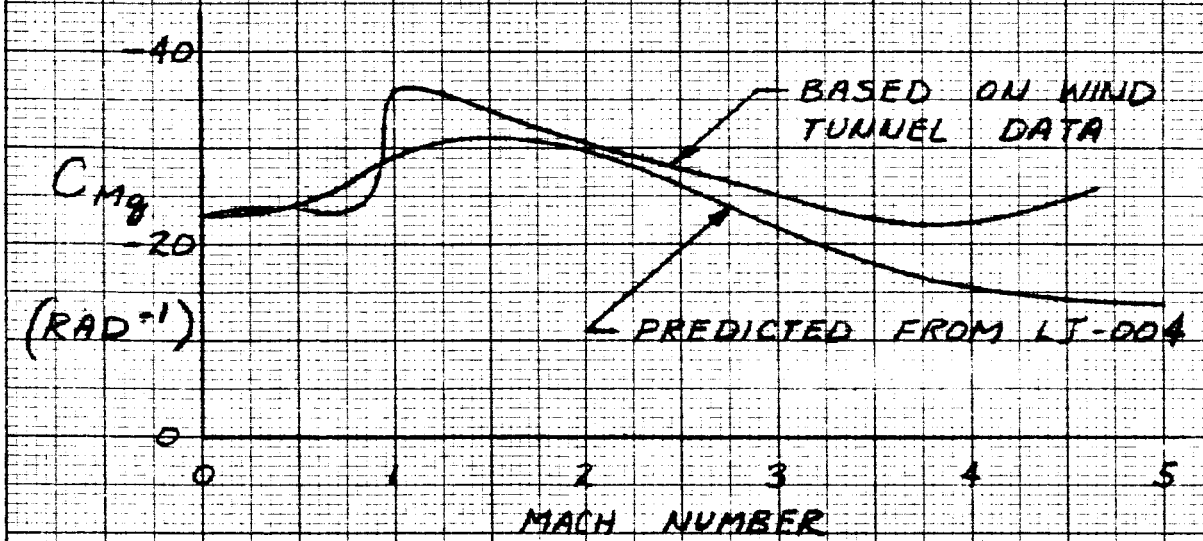




[redacted]

# LITTLE JOE II
## PITCHING MOMENT DUE TO PITCH RATE
## (COMPLETE CONFIGURATION)

FIGURE 23

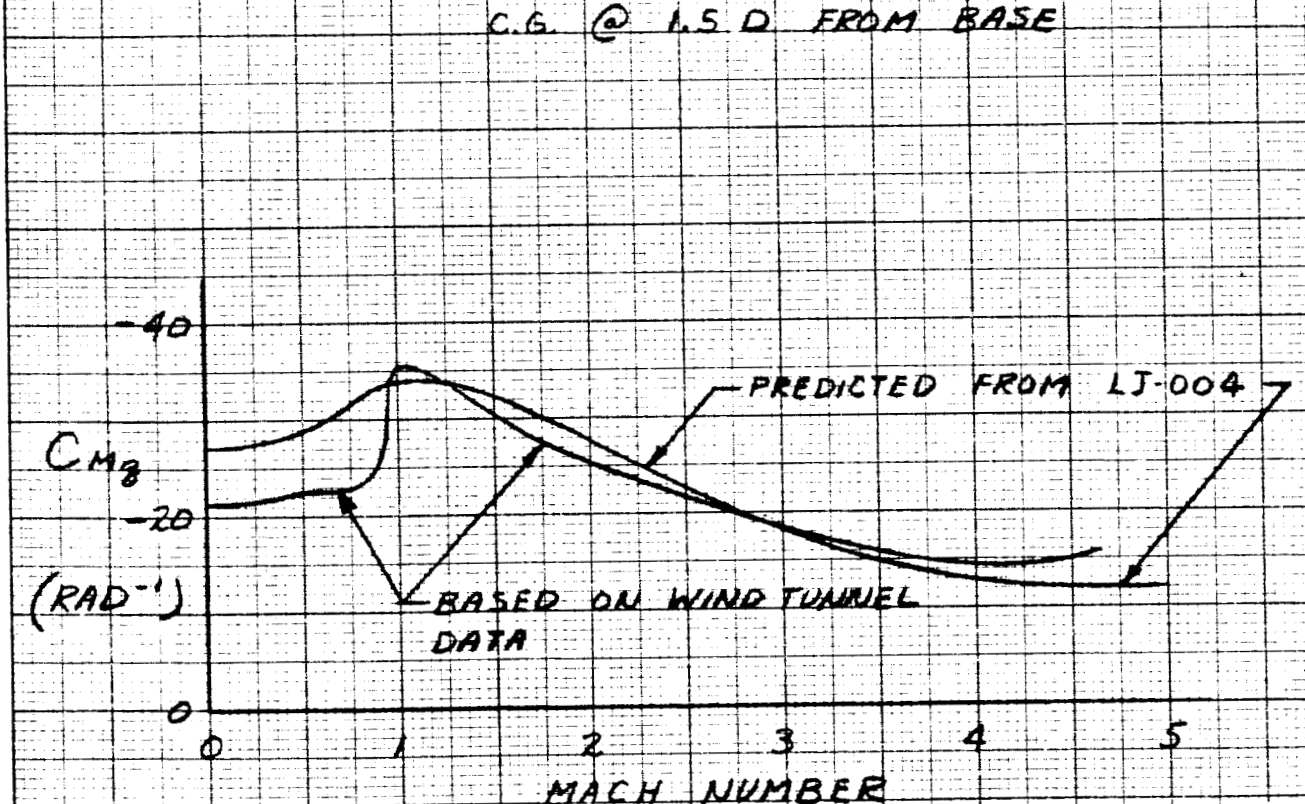

# LITTLE JOE II
## PITCHING MOMENT DUE TO PITCH RATE
## (COMPLETE CONFIGURATION)

FIGURE 24

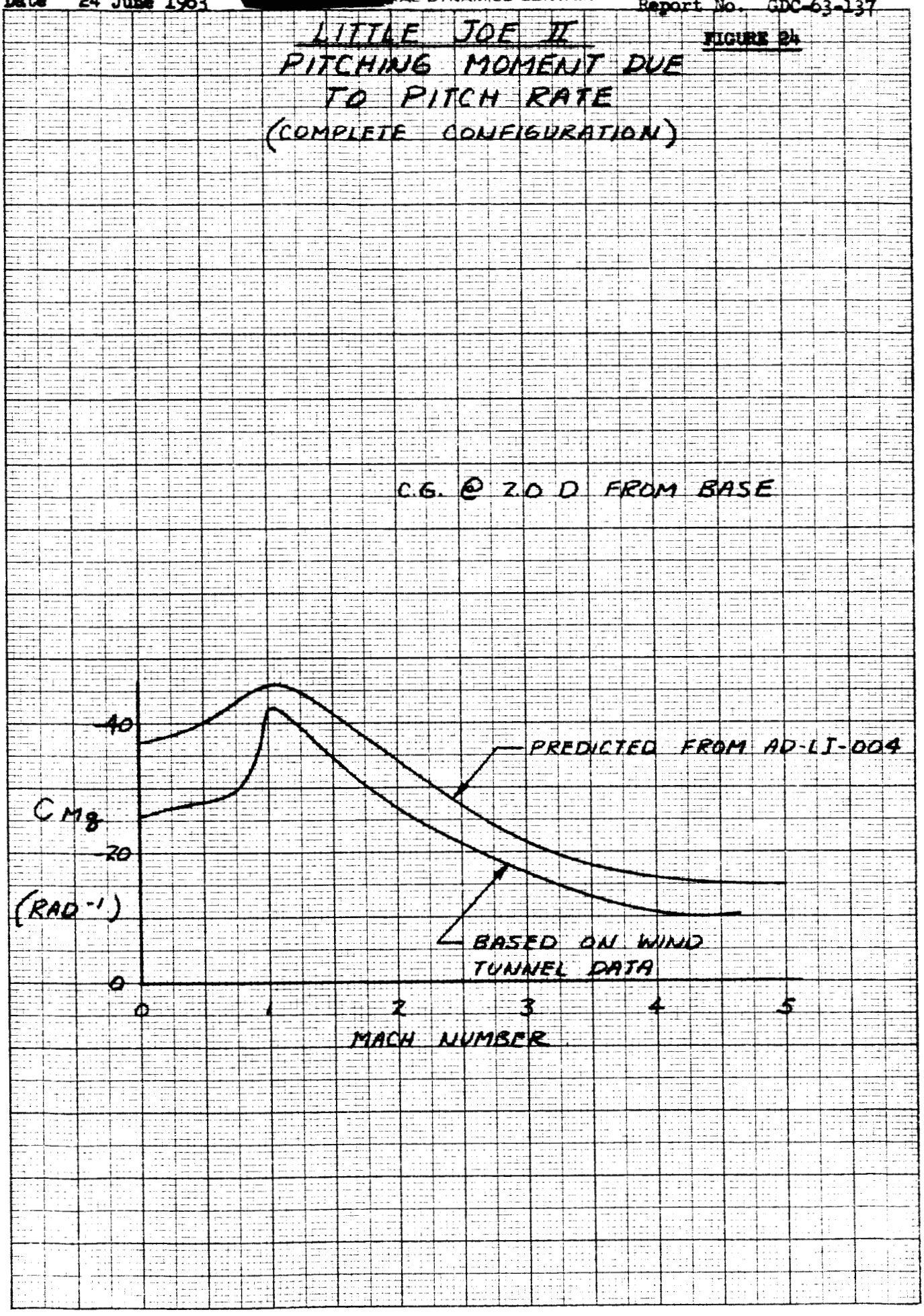

# LITTLE JOE II
## PITCHING MOMENT DUE TO PITCH RATE
## (COMPLETE CONFIGURATION)

FIGURE 25

160 INCH SERVICE MODULE
$S_{FIN}$ = 50 SQUARE FEET

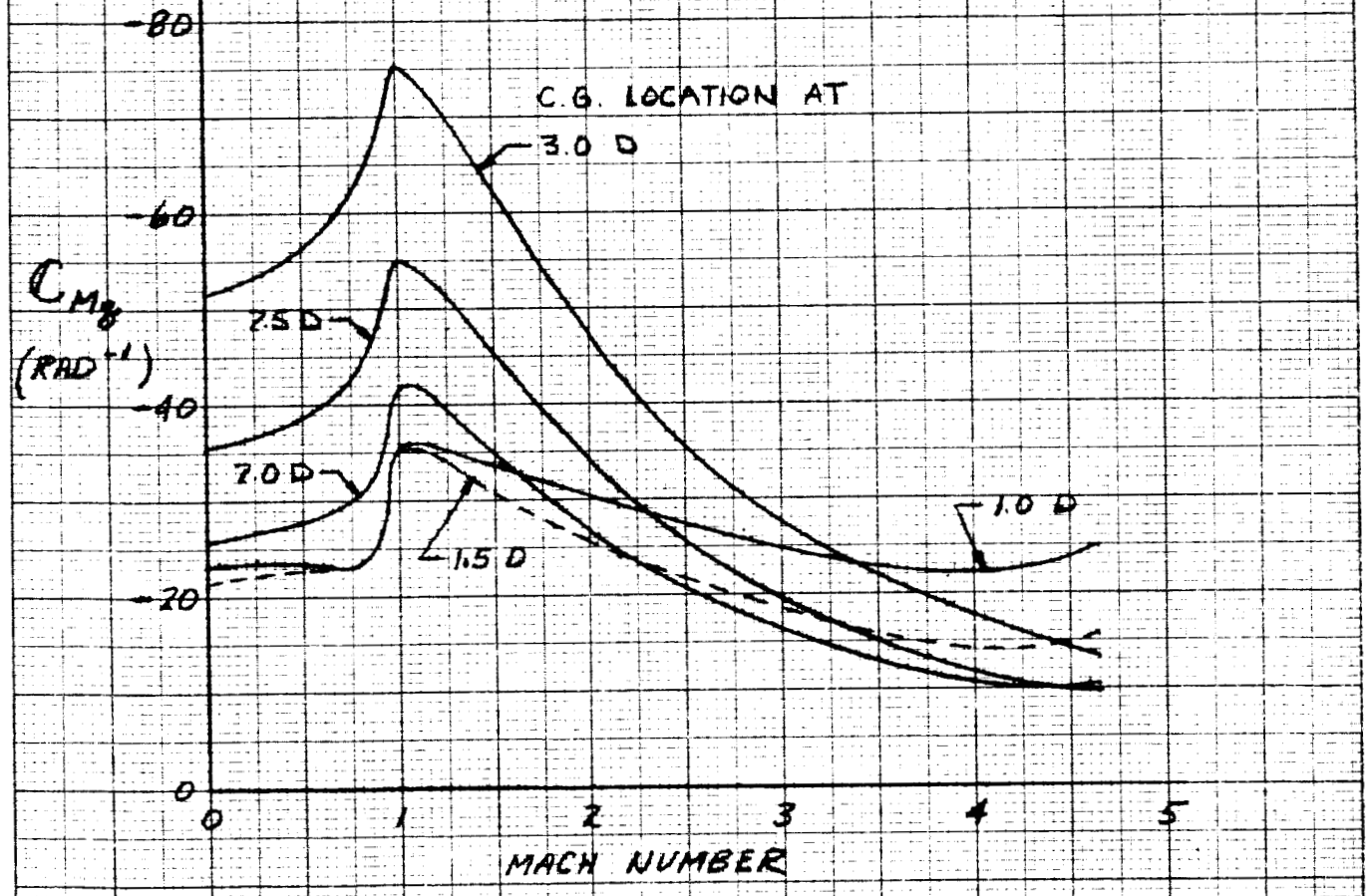

# LITTLE JOE II

FIGURE 26

## COMPARISON OF PRIMARY AND SECONDARY CONFIGURATIONS (COMPLETE CONFIGURATION)

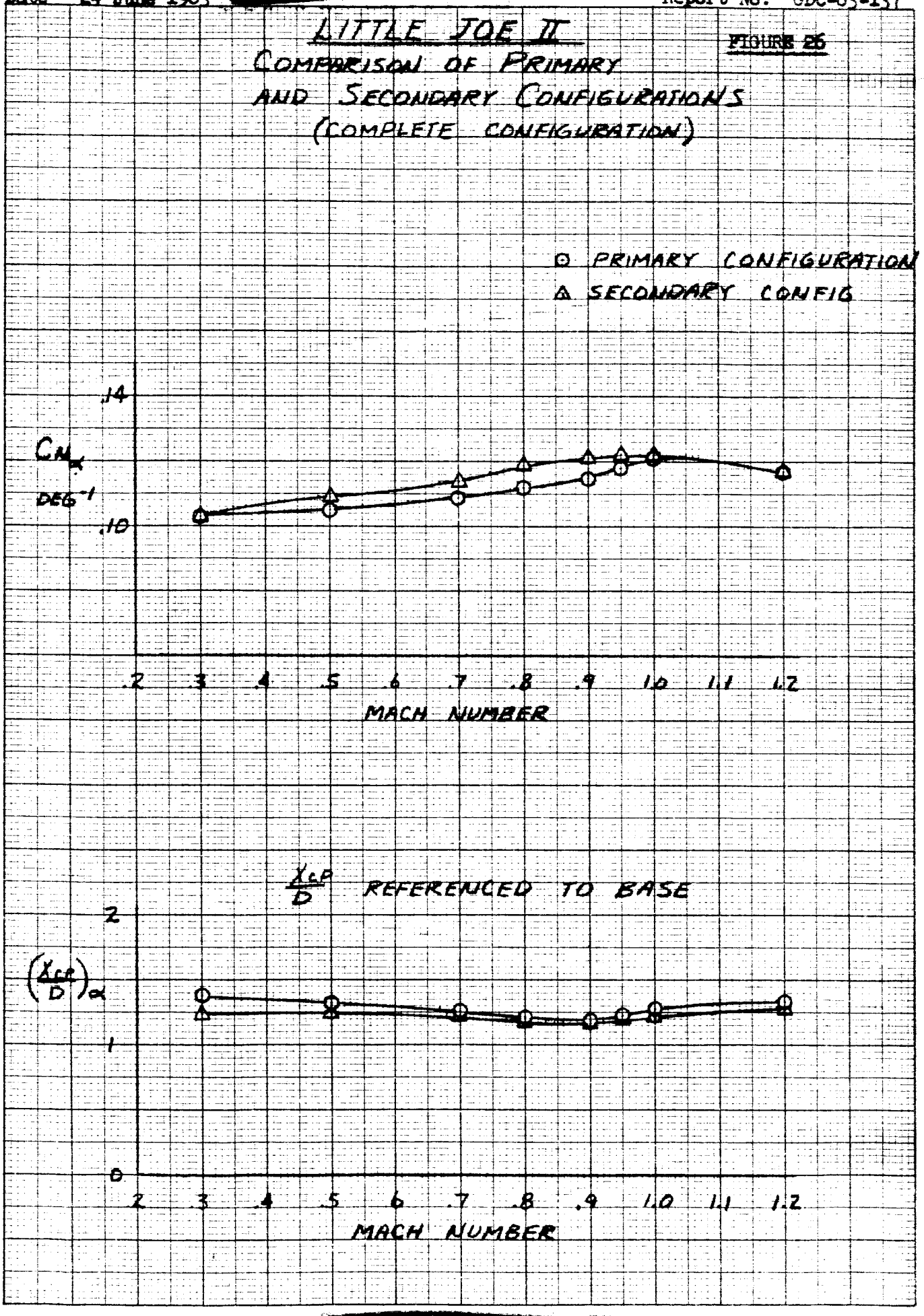




[redacted]

# LITTLE JOE II

FIGURE 27

## COMPARISON OF PRIMARY AND SECONDARY CONFIGURATIONS (COMPLETE CONFIGURATION)

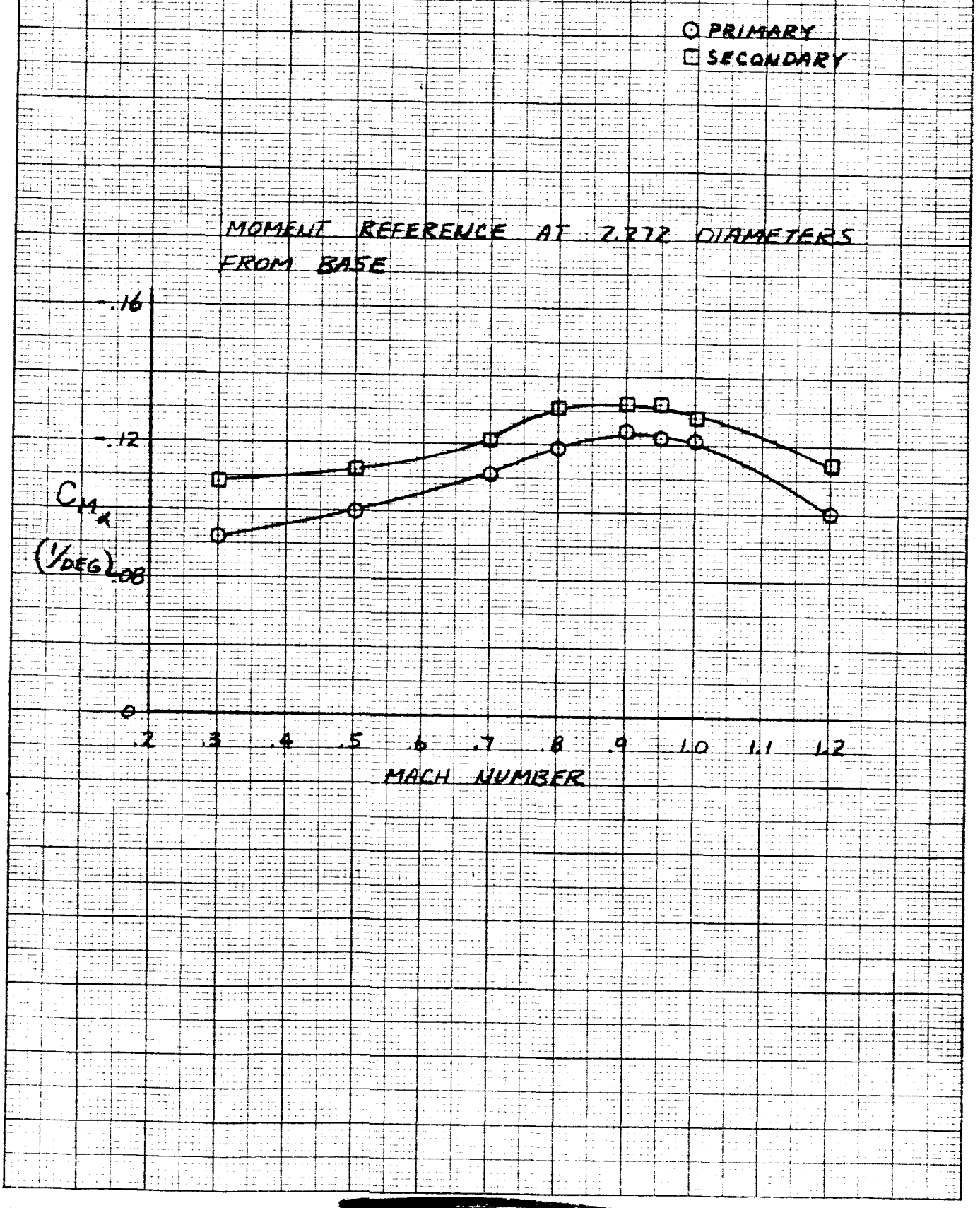

# LITTLE JOE II

FIGURE 28

## EFFECT OF REACTION CONTROL FAIRINGS ON NORMAL FORCE AND CENTER OF PRESSURE LOCATION

COMPLETE CONFIGURATION WITH 160 INCH SERVICE MODULE AND 50 SQ FT FINS

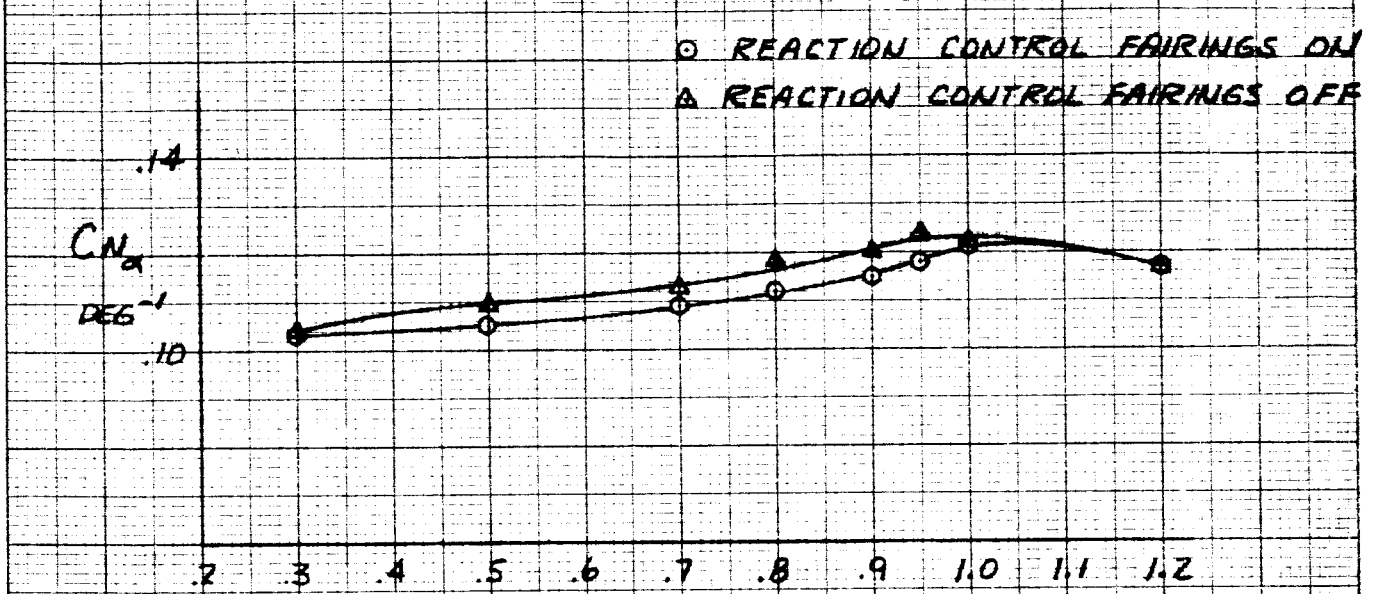


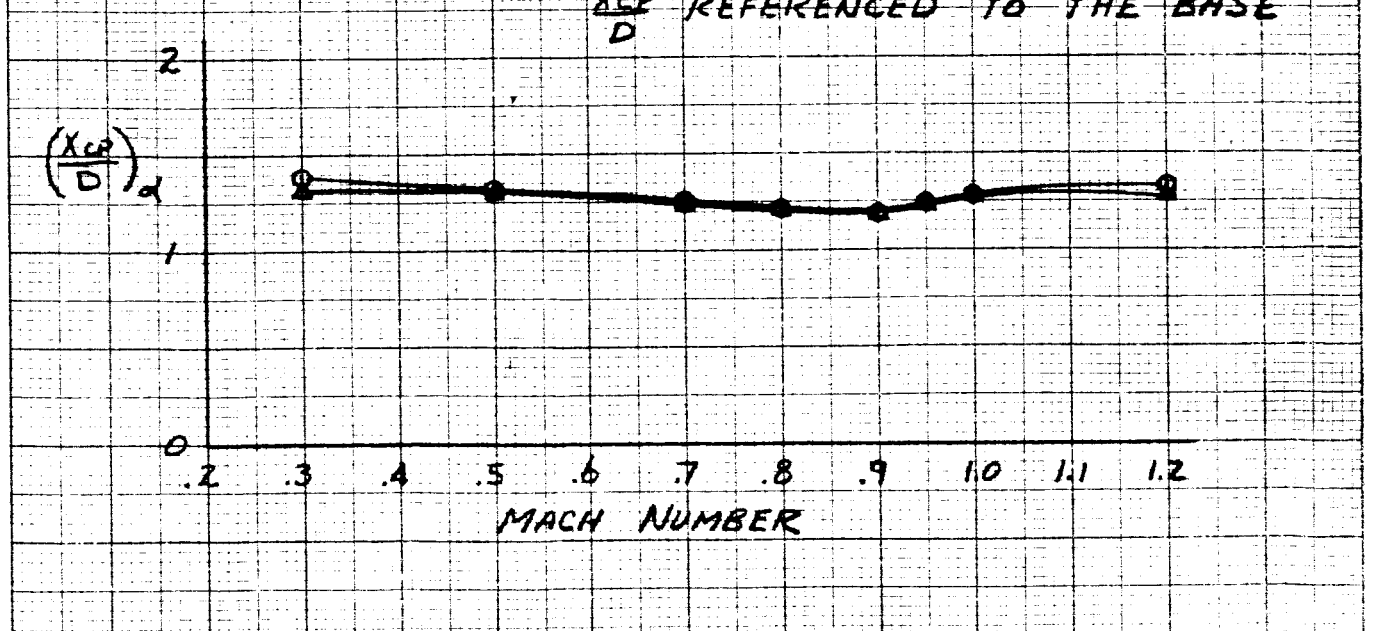

# LITTLE JOE II

FIGURE 29

## CONTROL HINGE MOMENTS

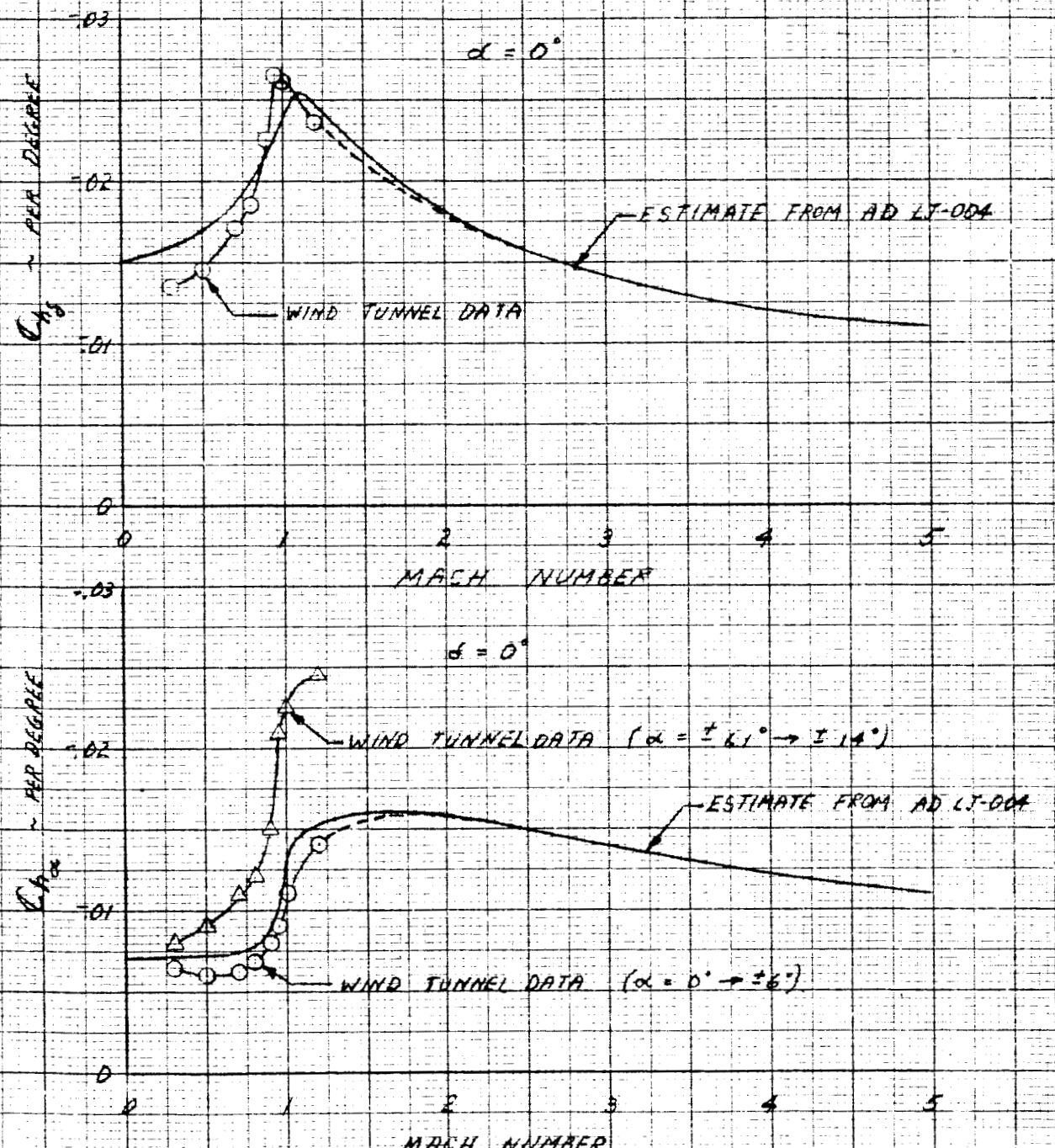

# LITTLE JOE II

FIGURE 30

## NORMAL FORCE AND CENTER OF PRESSURE LOCATION DUE TO ANGLE OF ATTACK (BODY ALONE)

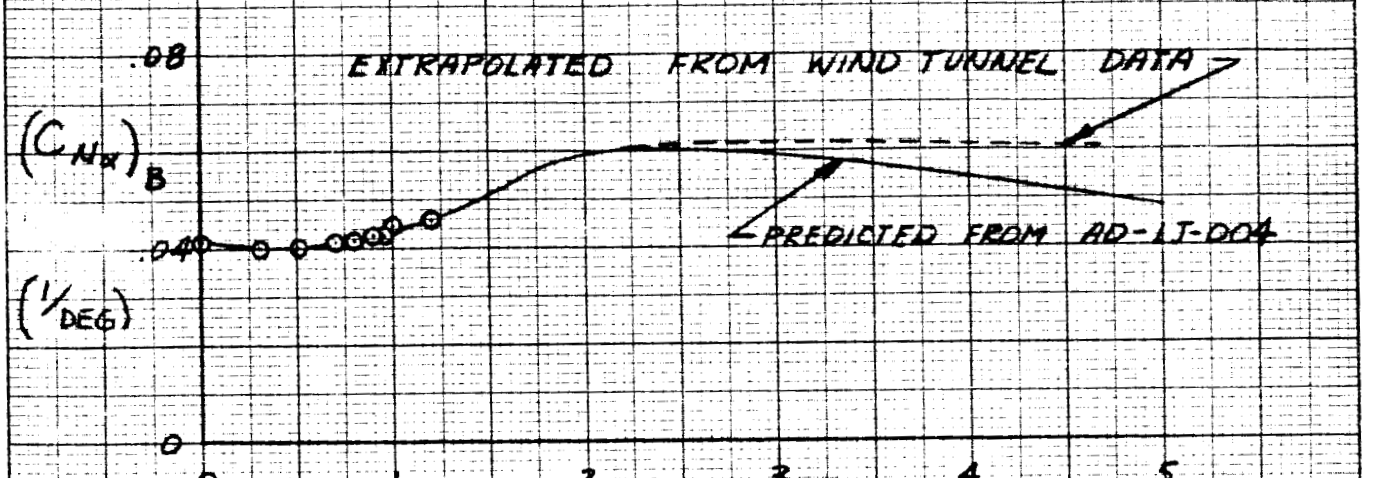


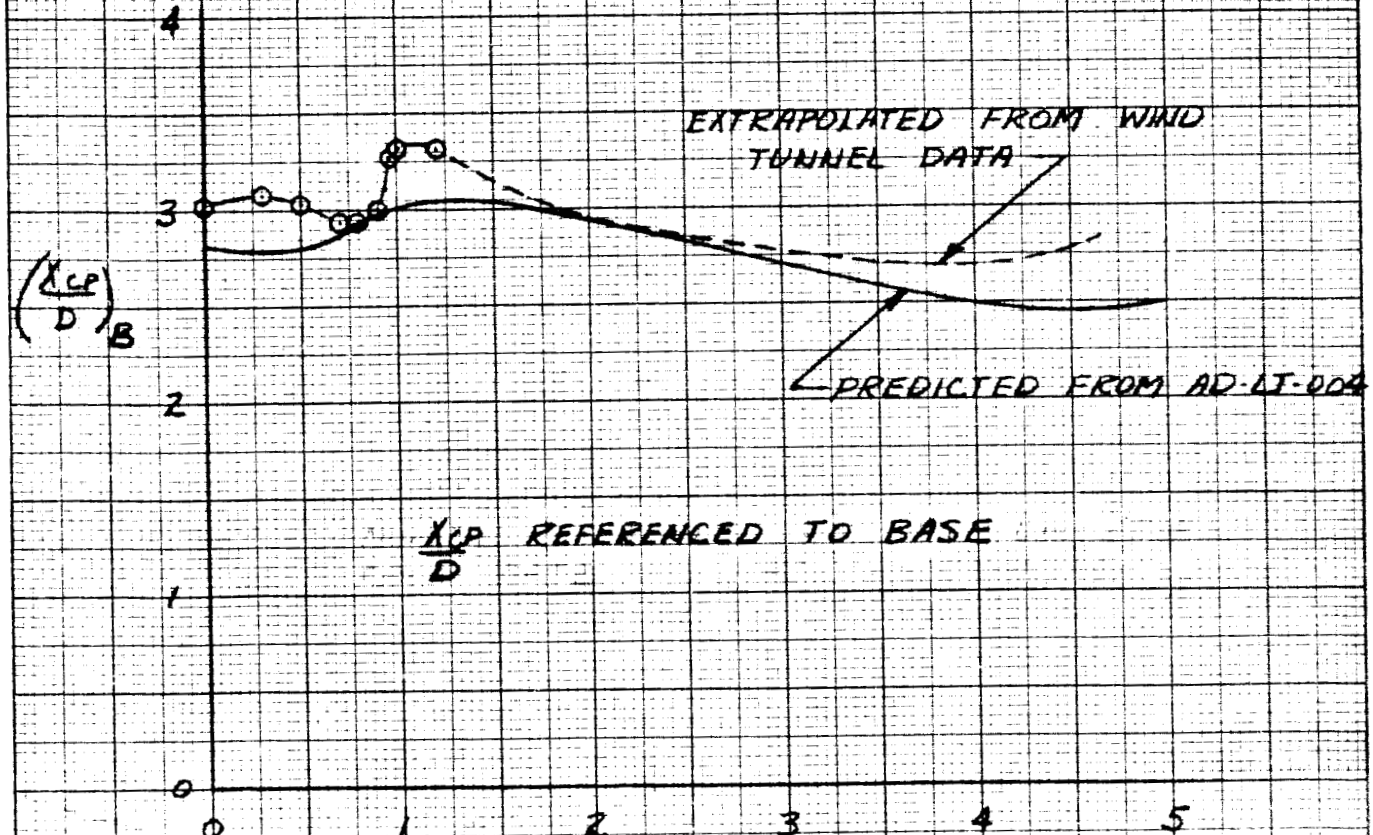

# LITTLE JOE II
## PITCHING MOMENT DUE TO ANGLE OF ATTACK (BODY ALONE)

FIGURE 31

MOMENT REFERENCE 2.272 DIAMETERS FROM BASE

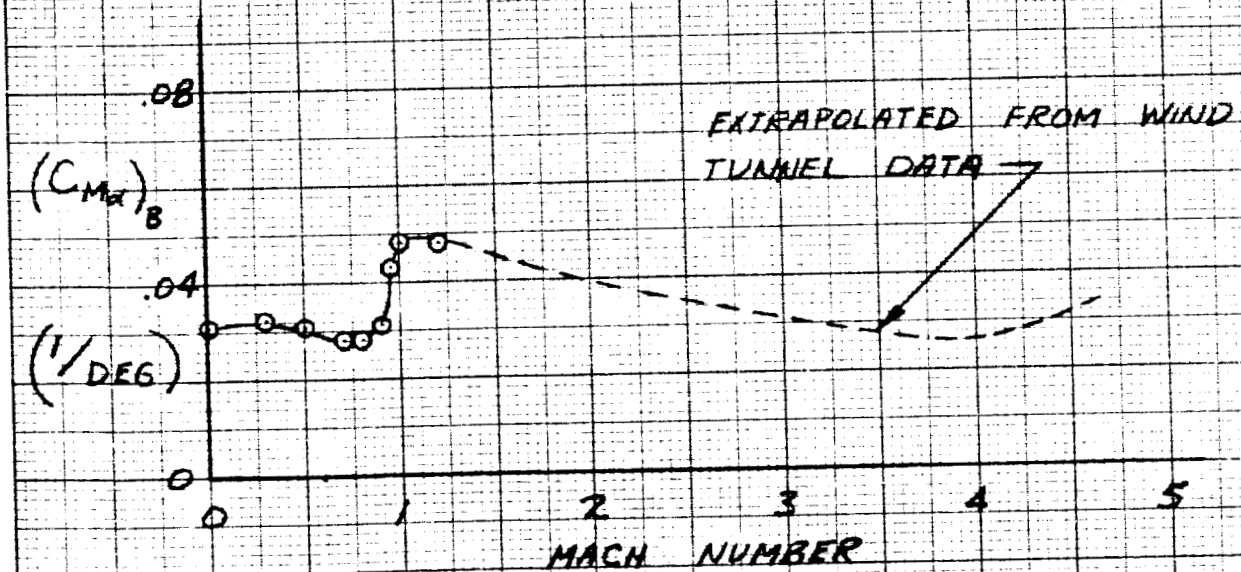

# LITTLE JOE II
## NORMAL FORCE AND CENTER OF PRESSURE LOCATION DUE TO ANGLE OF ATTACK (FINS ALONE)

FIGURE 32

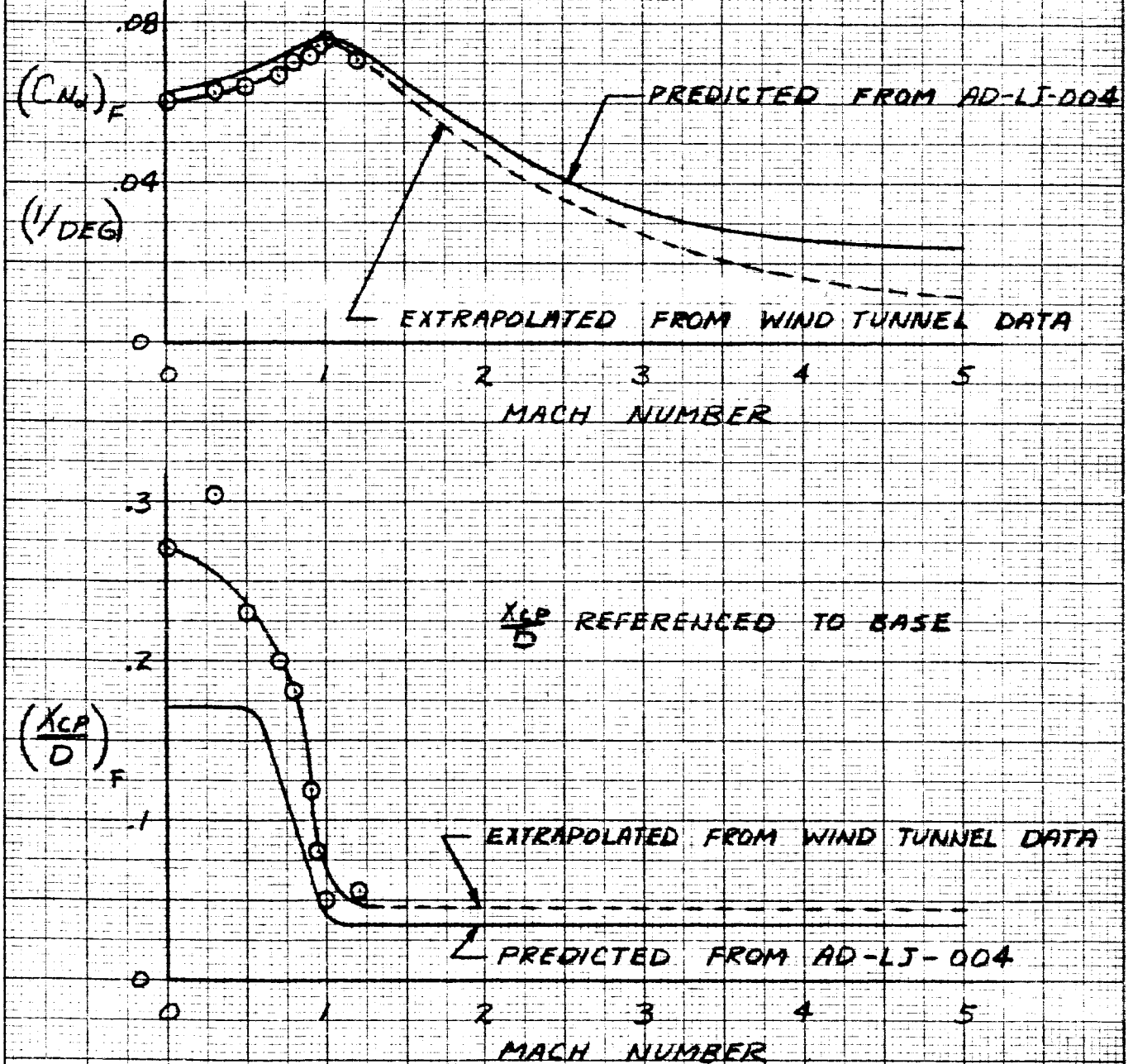

[redacted]

# ADDENDUM A

## EXHAUST JET PLUME EFFECTS

### INTRODUCTION

This addendum presents the results of a study to determine whether or not Little Joe II stability and control characteristics are adversely affected at high altitudes where billowing of the rocket exhaust jets might induce flow separation over the afterbody and fins.

A preliminary study of this problem was made during the early design stage of the vehicle and the results are reported in Reference 1. The present study is a follow-on to the original work. It was considered necessary to continue the analysis for the following reasons:

(a) Mission profiles and firing orders are now different from those evaluated in the original study.

(b) At the time of the original study it was assumed that the nozzle exits were in the plane of the vehicle's base, since detail design of this area had not yet been completed.

(c) The original analysis of size and shape of the jet plume was based on the methods given in Reference 2. It was necessary to extrapolate to much higher nozzle exit to ambient pressure ratios than those considered in Reference 2 when these techniques were applied to the Little Joe II configuration. More recent work, presented in Reference 3, enables the plume shape to be calculated for the actual nozzle pressure ratios encountered during the Little Joe II mission profile.

### ROCKET AND MISSION CHARACTERISTICS

For this study, the following nozzle and Algol rocket characteristics were used:

chamber pressure, $P_c$ = 429 psia

exit pressure, $P_e$ = 16.15 psia

exhaust gas specific heat ratio, $\gamma_j$ = 1.17

exit Mach number, $M_j$ = 2.68

nozzle exit angle, $\theta$ = 17°

[redacted]

[redacted]

At this time, mission (e) profile (high altitude abort) produces the highest altitudes and, consequently, largest jet plumes. As was pointed out in Reference 1, large jet plumes cause the boundary layer to separate because it cannot withstand the adverse pressure gradients associated with the large turning angle near the plume.

Representative flight conditions chosen for analysis from the mission (e) flight profile are as follows:

| Time From Launch (Seconds) | M | h (1000 ft) | $P_e/P_\infty$ |
|---|---|---|---|
| 50 | 2.16 | 55 | 12.1 |
| 60 | 2.84 | 79 | 38.2 |
| 70 | 3.65 | 111 | 163.1 |
| 80 | 4.67 | 155 | 897 |
| 86.5 | 5.02 | 189 | 3230 |

## DISCUSSION

Using the methods given in Reference 3, jet plume shapes for the above flight conditions were calculated. The results are shown on Figure 1, in which the radius of the jet plume is plotted versus axial distance (in nozzle radii) for both a quiescent atmosphere and the free stream Mach numbers listed in the above table. Turning angles of the free stream aft of the base were obtained from Reference 4; these angles established the points at which the free stream intersected the jet plume boundaries.

After the jet plume shapes have been established, it is necessary to determine the maximum pressure rise that can be tolerated before separation occurs. References 4, 5, and 6 contain experimental data which were used as a basis to establish the critical pressure coefficient for separation. The maximum allowable turning angles corresponding to the critical pressure coefficients were determined for each flight condition. The critical angles were exceeded at each of the flight conditions, indicating that separated regions exist. With flow deflection angle and shock angle determined by the critical pressure coefficient, the position of initial separation was determined using the experimental data from References 4 and 7 as a guide. It was found that the initial separation point would be aft of the base for flight conditions at 2.16, 2.84 and 3.65 Mach numbers. At M = 4.67 and 5.20 there are separated regions on the afterbody, but the fins are not affected (see Figure 2).

[redacted]

[redacted]

## CONCLUSIONS

From the foregoing discussion it is concluded that jet billowing of the underexpanded nozzles will not cause any stability and control problems on Little Joe II.

[redacted]

[redacted]

REFERENCES

1. Wener, N. L., "Attitude Control System Study NASA Project Apollo Test Launch Vehicle - Little Joe II," GDC/62-190, 2 July 1962.

2. Love, E. S., Grigsby, C. E., Lee, L. P. and Woodling, M. J., "Experimental and Theoretical Studies of Axisymmetric Free Jets," NASA Technical Report R-6, 1959.

3. Henson, J. R. and Robertson, J. E., "Methods of Approximating Inviscid Jet Boundaries for Highly Underexpanded Supersonic Nozzles," AEDC-TDR-62-7, May 1962.

4. Hargis, C. B., Davison, P. H. and Savage, S. B., "Methods for Estimating Base Pressures on Aircraft Configurations." WADC Technical Note 57-28, July 1957.

5. Kuehn, D. M., "Experimental Investigation of the Pressure Rise Required for the Incipient Separation of Turbulent Boundary Layers in Two-Dimensional Supersonic Flow." NASA Memo 1-21-59A, February 1959.

6. Chapman, D. R., Kuehn, D. M. and Larson, H. K., "Investigation of Separated Flows in Supersonic and Subsonic Streams with Emphasis on the Effects of Transition." NACA Report 1356, 1958.

7. Fetterman, D. E., "Effects of Simulated Rocket-Jet Exhaust on Stability and Control of a Research-Type Airplane Configuration at a Mach Number of 6.86." NASA TM X-127, October 1959.

[redacted]

FIGURE A-1

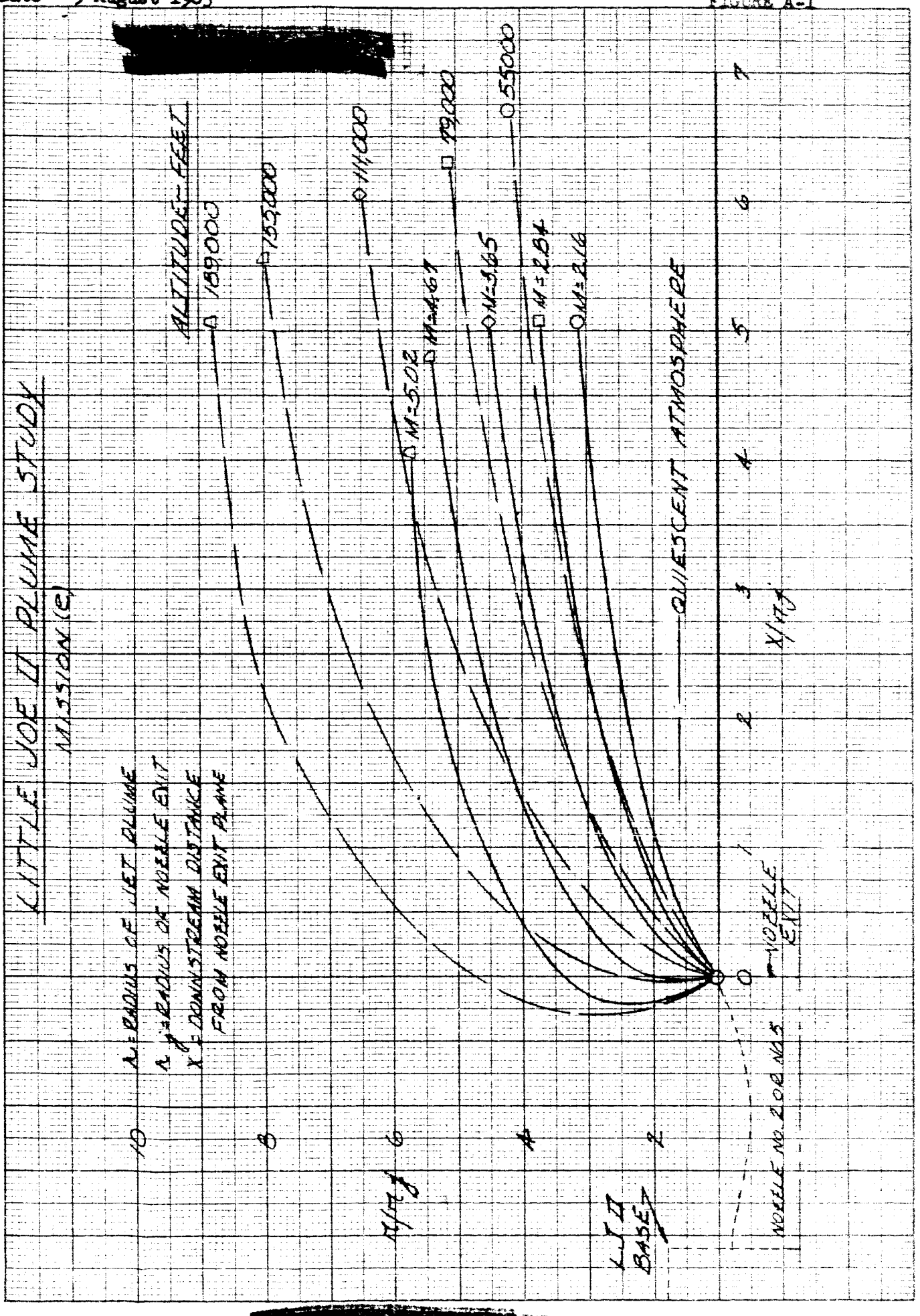
LITTLE JOE II PLUME STUDY
MISSION (2)
ALTITUDE - FEET
189000
153000
114000
79000
55000
M=5.02
M=4.67
M=3.65
M=2.84
M=2.46
QUIESCENT ATMOSPHERE
X/R_T
R/R_T
NOZZLE EXIT
NOZZLE NO. 2 OF NAS
LJ-2 BASE
A = RADIUS OF JET PLUME
R = RADIUS OF NOZZLE EXIT
X = DOWNSTREAM DISTANCE FROM NOZZLE EXIT PLANE

FIGURE A-2

[redacted]

[redacted]